ANL/CP--75512

DE93 005324

48

STRUCTURAL FAILURE ANALYSIS OF REACTOR VESSELS

by

P. A. Pfeiffer

Reactor Engineering Division
Argonne National Laboratory
9700 South Cass Avenue
Argonne, IL 60439

Abstract

Maintaining structural integrity of the reactor vessel during a postulated core melt accident is an important safety consideration in the design of the vessel. This study addresses the failure predictions of the vessel due to thermal and pressure loadings from the molten core debris depositing on the lower head of the vessel. Different loading combinations were considered based on a wet or dry cavity and pressurization of the vessel based on operating pressure or atmospheric (pipe break). The analyses considered both short term (minutes) and long term (days) failure modes after the core has melted. Short term failure modes include creep at elevated temperatures and plastic instabilities of the structure. Long term failure modes are caused by creep rupture that lead to plastic instability of the structure. Based on these studies, the analyses predict the reactor vessel examined will remain intact after the core melt has deposited on the lower vessel head.

1. Introduction

The paper addresses the failure prediction of the vessel due to thermal and pressure loadings from molten core debris. The core debris are collected on the bottom head of the reactor vessel. The finite element computer program STRAW was employed to perform structural analyses of common reactor vessels. STRAW (Schoeberle, et al., 1974; Kulak, et al., 1978; Schreyer, et al., 1983) is a nonlinear structural-fluid and thermomechanical finite element program.

Structural failure can occur by two mechanisms. They are plastic instability of the structure and creep rupture. Plastic instability occurs through thermal degradation of the elastic-plastic stress-strain response. Essentially the effective stress state becomes larger than the saturation (ultimate) stress. This causes the stress-strain response to become unstable (i.e., equilibrium is unobtainable). Creep rupture is the final stage of a metal material being exposed to a long-time loading of stress at an elevated temperature. When a load that is less than the ultimate load is applied to a metal at room temperature, the material deforms relatively rapidly to equilibrium point, and then the deformation remains constant with time. When a load is applied to a metal at an elevated temperature, the material likewise deforms rapidly at first but then continues to deform, or creep at a much slower rate. This is called primary and secondary

---

creep; in primary creep the strain increases at a decreasing rate and in secondary creep the strain increases at a nearly constant rate. The final stage is when the strain increases at an increasing rate up to failure. The failure, or creep rupture load is less than the load that would cause failure at that elevated temperature in a short-time loading test. Creep is included in the elastic-plastic analysis by adjustment of the yield and saturation (ultimate) stress. Adjustment of the saturation stress is based on the strain rate and temperature of the material. Primary and secondary creep is modeled through the creep constitutive relationship. Creep rupture is modeled through a Larson-Miller creep rupture curve (Larson and Miller, 1952) and damage is accumulated through a "life fraction" relationship based on the stress and temperature of an integration point through time in the structure.

2. Reactor Vessel Models

All analyses of the reactor vessels were axisymmetric. The reactor vessel model includes the cylindrical shell and torispherical lower head which is welded to the cylindrical shell. The lower head itself is comprised of a hemispherical portion which is welded to a partial toroidal section. All penetrations were neglected in the model. The cylindrical component is 280.1 in. in total length with a centerline diameter of 241.0 in.; the lower head has a radius of 224 in. for the hemispherical portion and a radius of 44.3 in. for the partial toroidal section. Wall thicknesses of 2.0 in. and 2.5 in. were analyzed. The upper part of the cylindrical component is welded to 14 in. flange that is 10 in. in thickness. The reactor vessel head closure is supported by this flange. The head closure is a 17.0 in. thick plate with many penetrations. These components are constructed of Type 316 stainless steel. Seventy-two, 2-¾ in. diameter bolts secure the closure head to the cylindrical shell. The bolts are constructed with SA540 grade B23 alloy steel. A schematic of the reactor vessel is shown in Figure 1.

3. Material Properties of 316 Stainless Steel

A viscoplastic constitutive model for 316 stainless steel was used to model the stress-strain behavior and creep response. This model was developed by Dimelfi and Kramer (1980) and uses a Voce equation with a flow stress formulation. The plastic flow behavior of annealed, unirradiated type 316 stainless steel is described by the Voce equation, which has the form of

$$\sigma = \sigma_s - (\sigma_s - \sigma_y) \exp\left(-\varepsilon_p/\varepsilon_c\right) \tag{1}$$

where σ_y is the yield stress of fully annealed, unirradiated material; and σ_s is the saturation stress approached by the flow stress σ as ε_p increases. The quantity ε_p is the hardness parameter which is equal to the accumulated plastic strain. It is assumed to represent other positive and negative contributions to the strength, as well, such as prior cold work, irradiation hardening, and softening due to annealing. Since σ_s, σ_y and ε_c are related to the initial work-hardening rate, which is insensitive to temperature and strain rate, only σ_s and σ_y are independent material parameters with ε_c being dependent on σ_s and σ_y. Both σ_s and σ_y are temperature and strain rate

dependent functions chosen so that at low strain rate, Eq. 1 reduces to the familiar power law of thermally activated creep. Details of these functional dependencies are summarized in the appendix of Dimelfi and Kramer (1980).

In the above viscoplastic model, creep can occur only after the effective stress becomes larger than the yield stress and plastic strain initiates. Since the yield stress at high temperatures (>1000 F) is based on very high strain rates, creep can only occur in the model after the yield stress is reached. Thus, the stress-strain response up to the yield stress at high temperatures are inaccurate at low strain rates because of the reduction in yield stress. The viscoplastic model was modified to include a pseudo viscoelastic response. This was accomplished by using the elastic strain rate response and adjusting the yield stress based on the strain rate and temperature. This modification is only important when assessing the structural response under loadings that do not cause significant plastic strains or damage.

The temperature dependent material properties are given in Figs. 2 through 4 for the Young's modulus, yield stress and saturation (ultimate) stress, respectively. Above 2500°F the material is assumed to have melted and essentially gives a zero stress response to any strain value. The values of Poisson's ratio equal to 0.3 and coefficient of thermal expansion equal to 11×10^{-6} in/in/°F were used and both are assumed to be temperature independent. Uniaxial true stress-true strain curves were obtained with the viscoplastic model. Figure 5 depicts the true stress-true strain response for various temperatures of 100°F, 1200°F, 1800°F, and 2400°F. For each temperature, different strain rates of 13.3, 0.133, 0.133, 1.33×10^{-4} and 1.11×10^{-7} in/in-sec were given to indicate the relative degree of strain-rate sensitivity. The higher the strain-rate sensitivity (i.e. reduction in strength), the higher the creep response will be. Below 1000°F there is no strain-rate sensitivity and thus little or no creep response. As temperatures approach the melting temperature of 2500°F, strain-rate sensitivity and creep accelerate. Note that at high strain rates (>10 in/in-sec) the yield stresses and saturation stresses in Fig. 5 asymptotically approach the values given in Figs. 3 and 4 for yield stress and saturation stress, respectively. Thus for high strain rates the creep effect is reduced.

Failure due to creep rupture at various temperatures is given in Fig. 6 for stress levels versus time to rupture. The curve fits are based on creep rupture data for Larson and Miller (1952) and Department of Defense (1986) for 18-8 Cr-Mo stainless steel. The time to rupture, t(hr) is based on a Larson-Miller parameter equation and is solved for the rupture time and results in:

$$t = 10^{\left[(C_1 \log_{10} \sigma + C_2)/T - 20\right]} \qquad (2)$$

where σ is the stress level, T is the absolute temperature in °R and C_1 and C_2 are constants dependent on the stress level. The values of C_1 and C_2 based on the stress level are

$C_1 = -62482.9,\ C_2 = 331828$ $\quad \log_{10}\sigma \geq 4.82$

$C_1 = -17615.4,\ C_2 = 115556$ $\quad 4.3 \leq \log_{10}\sigma < 4.82$

$C_1 = -11745.7,\ C_2 = 90326.5$ $\quad 3.433 \leq \log_{10}\sigma < 4.3$

$C_1 = -7134.0,\ C_2 = 74493.1$ $\quad \log_{10}\sigma < 3.433$

Under constant stress and temperature the time to failure can easily be established. However, since most structural elements are not subjected to either constant stress or constant temperature, a creep-rupture damage criteria is needed to predict time to rupture. One method is the "life fraction" rule based on the premise that the expenditure of each individual rupture life fraction of the total life at elevated temperature is independent of all other fractions of the life to rupture, and that when the fractional life used up at different stress levels and temperatures is added up, it will equal unity; which is

$$\sum \frac{t_i}{t_{Ri}} = 1 \qquad (3)$$

where t_i is the time at temperature i and t_{Ri} is the creep rupture time at temperature i. The creep rupture values in Fig. 6 are based on tensile tests. There is some debate on whether or not creep rupture is valid for compressive stresses. In this study it is assumed that with compressive stresses, a lateral tensile stress will develop and creep rupture will occur. When rupture does occur, the stresses in the element are set to zero and no load can be carried.

4. Loading Cases

A failure analysis of different thermal and pressurizations were investigated. Two thermal load cases were utilized and are obtained from a core melt on the bottom head. The first thermal load case was obtained from nucleate boiling heat transfer on the bottom head. A steady state temperature distribution is obtained in about ten hours (35285 sec) after the melt comes in contact with the bottom head. The temperature distribution is given in Figure 7. The second thermal load case was obtained from film boiling heat transfer on the bottom head. A steady state temperature distribution is obtained after about 111 minutes. The temperature distribution is based on a heat transfer coefficient of 50 BTU/hr-ft^2-F on the outside of the vessel and is given in Figure 8.

Two pressure cases were considered for each thermal case. The first case is an internal loading of 75 psi based on the operating pressure of the system. The second case is an internal loading pressure of 0 psi assuming a pipe break and thus relieving the internal pressure.

Other loadings on the vessel wall include the melt mass and the outer cavity water head. The water level of the cavity is indicated in Figure 1. The maximum outer water pressure on the reactor vessel is about 8.7 psi at the center of the bottom head. The outer cavity water head is present for the first thermal load case only. In the second thermal load case, a dry cavity was assumed.

5. Numerical Simulations

Nodalization of the reactor vessel model is given in Figure 9. The model is comprised of thirty-two nodes and thirty-one axisymmetric shell elements. Each shell element has ten gaussian integration points, five through the thickness and two sets along the length. The locations of the integration point, are based on a Gaussian integration. The closure head and upper flange were not modeled because they are in the far-field from potential failure locations. Thus, the top node 32 was assumed to be fixed against translation and rotation.

Four different analyses were performed and are listed in Table 1.

Table 1. Analyses Performed

Load Case	Bottom Head Heat Transfer	Internal Pressurization (psi)	Wall Thickness (in)	Water in Cavity *
1	Nucleate Boiling	75	2	Yes
2	Nucleate Boiling	0	2	Yes
3	Film Boiling	75	2.5	No
4	Film Boiling	0	2.5	No

*For purposes of structural analysis only.

All the above simulations were assumed to have a static behavior with no dynamic loading response. A total simulation time of 240 hrs. was computed with 2400 time steps of 360 sec each. Static equilibrium was checked by an error force balance norm (internal force minus external force) of 1% and an energy error balance norm (error force multiplied by change in displacement) of 1.0×10^{-4}% of the total strain energy of the structure. These two criteria assure that at each time step the model was in static equilibrium.

6. Results

A. Thermal Load Case One

The temperatures at the gauss points of the finite element mesh are given in Fig. 10. The arc length is 0 m at node 1 and 10.9 m at node 32 of the mesh shown in Fig. 9. Each layer is shown with layer 1 being near the outside of the vessel and layer 5 being near the inside of the vessel. Initially the whole vessel is assumed to be at 150 F operating temperature. Mesh displacement plots for load cases 1 and 2 are given in Figure 11. The dashed lines indicate the original position (undeformed) of the mesh. In both load cases the vessel remains intact up to at least 240 hours. The plastic strains that arise at 240 hours are shown in Figs. 12 and 13 for load cases 1 and 2 respectively. The largest plastic strain is about 2.4% at a temperature of 2012°F (1100 C). At this temperature the failure strain is estimated to be 30%, thus the lower head is plastically stable, and failure of the vessel due to plastic instability will not occur. Steady state thermal conditions were assumed up to 240 hours. In reality the pool will begin to cool after a few hours from the initial formation. As the pool begins to cool, the potential failure of plastic instability in the vessel head will be mitigated.

Two types of creep behavior are present in the vessel due to the thermomechanical loadings. At elevated temperatures the deformation of the vessel continues with no increase in the loading (i.e. internal pressure, core melt weight, and water cavity pressure remain constant in time). This is called creep and is defined as the time-dependent inelastic deformation of materials. Secondly, stress relaxation is the relief of stress as a result of creep. This is characterized by the reduction of stress with time while the total deformation remains constant (i.e. steady state imposed thermal strains). Stress relaxation continues until an asymptotic residual stress is reached with the secondary creep rate being very small.

The vertical displacement of the vessel at the bottom center is shown in Figure 14 for both pressures. The displacement plots indicate both primary and secondary creep behavior after a steady state thermal condition is reached at ten hours. An indication of relative failure based on creep rupture is depicted in Figure 15 for both pressures. This figure shows the creep rupture accumulation based on the stress and temperature history near the most critical location of the vessel. The location is at the bottom center of the vessel at the inner most layer (layer 5, inside of vessel wall). At the end of 240 hours, the layer has used about 33% of its life for both load cases. The life term is based on the failure time predicted by the Larson-Miller creep rupture for 316 stainless steel. Figures 16 and 17 show the creep rupture values at 240 hours for the entire vessel for load cases 1 and 2, respectively. An estimation of the time to failure of the vessel based on creep rupture can be made at the critical location (i.e. highest creep rupture values). The estimated time to failure for each layer based on the stress levels at ten hours (initial steady state thermal conditions reached) and at 240 hours for load cases 1 and 2 are given in Tables 2 and 3, respectively.

Table 2. Load Case 1 Rupture Times

Values at 10 Hours				
Layer	Stress (psi)	Temperature (°C)	Life Fraction	Time to Rupture (Hr)
1	43511	149	0.0000	3.5×10^{24}
2	20523	342	0.0000	5.8×10^{15}
3	-16636	625	0.0000	1.6×10^{5}
4	-3303	908	0.0026	1105
5	-939	1101	0.0529	33
Values at 240 Hours				
1	31024	149	0.0000	9.1×10^{27}
2	9487	342	0.0000	2.4×10^{19}
3	-5730	625	0.0000	3.7×10^{8}
4	-849	908	0.0067	1.6×10^{5}
5	-234	1101	0.3299	1287

Table 3. Load Case 2 Rupture Times

Values at 10 Hours				
Layer	Stress (psi)	Temperature (°C)	Life Fraction	Time to Rupture (Hr)
1	42641	149	0.0000	5.7×10^{24}
2	6476	340	0.0000	1.9×10^{21}
3	-17912	621	0.0000	1.2×10^{5}
4	-3555	901	0.0031	1007
5	-1008	1092	0.0489	37
Values at 240 Hours				
1	30080	149	0.0000	1.8×10^{28}
2	-5010	340	0.0000	2.9×10^{22}
3	-6763	621	0.0000	1.4×10^{8}
4	-965	901	0.0074	1.4×10^{5}
5	-274	1092	0.3481	1128

The estimated times are based on the creep rupture time according to Fig. 6. The most significant result is that the stresses have been reduced substantially from ten hours to 240 hours. This occurs due to the stress relaxation of the thermal stresses. Thus the time to failure (i.e. creep rupture) is increased when the assessment is based on the stress levels at 240 hours. The times to failure for each layer are estimated because it is assumed the stresses remain constant. However, the results indicate that the stresses relax (i.e. stresses are not constant and reduce with time) and time to failure at 240 hours would be conservative. The stresses in the vessel wall will redistribute as the inner layers begin to fail from creep rupture. Since there is a variation of temperature through the wall, the thermal stresses in the remaining layers will decrease as the inner layers fail towards the outside of the vessel due to the bending moments that develop from the temperature gradient. This result was based on the assumption that the temperatures through the thickness remain the same after the layers have ruptured. The stresses that result from mechanical loadings (i.e. internal pressure, core melt weight and water cavity pressure) will increase the stresses in the remaining layers due to a reduced cross section. A simplified analysis of the vessel was performed in order to provide an estimation of the time to total structural failure. The analysis used large time steps to facilitate the long simulation time (up to thousands of years) needed to obtain failure. With these large time steps, the simulation of creep and stress relaxation in the vessel are approximate. This is because of the inaccuracies in the temporal integration of the creep response with large time steps. From the simplified analyses it was found that a conservative value of time to failure could be estimated from the stress levels at 240 hours based on the projected time to failure of the third layer. Thus for load case 1 the time to failure of the vessel would be 3.7×10^8 hours or about 42,000 years, assuming that the temperature field remains constant. Load case 2 has an estimated time to failure of the vessel of 1.4×10^8 hours or about 15,000 years. Obviously, the vessel will not fail due to creep rupture, because the pool will have cooled off in this time period.

B. Thermal Load Case Two

The temperatures of the gauss points of the mesh are given in Fig. 18. Initially, the whole vessel is assumed to be at 150 F operating temperature. Mesh displacements for load cases 3 and 4 are given in Fig. 19. In both cases, the vessel remains intact up to at least 240 hours. The plastic strains that develop at 240 hours are depicted in Figs. 20 and 21 for load cases 3 and 4, respectively. The largest plastic strain is about 1.6% at a temperature of 2062°F (1128 C). At this temperature the failure strain is estimated to be 30%, thus the lower head is plastically stable and failure of the vessel will not occur.

The vertical displacement of the vessel at the bottom center is shown in Fig. 22 for both pressures. The displacement plots indicate both primary and secondary creep behavior after a steady state thermal condition is read at about two hours. An indication of relative failure based on creep rupture is depicted in Fig. 23 for both pressures. This figure shows the creep rupture accumulation based on the stress and temperature history near the most critical location of the vessel. The location is at the bottom center of the vessel at the (layer 5, inside of the vessel wall). At the end of 240 hours, the layer has used about 90% of its life for load case 3. Figures 24 and 25 depict the creep rupture values at 240 hours for the entire vessel for load cases 3 and

4, respectively. An estimation of the time to failure of the vessel based on creep rupture can be made at the critical location (i.e. highest creep rupture values). The estimated time to failure for each layer based on the stress levels at two hours (initial steady state thermal conditions reached) and at 240 hours for load cases 3 and 4 are given in Tables 4 and 5, respectively.

Table 4. Load Case 3 Rupture Times

Values at 2 Hours				
Layer	Stress (psi)	Temperature (°C)	Life Fraction	Time to Rupture (Hr)
1	22539	592	0.0000	9.3×10^{4}
2	9754	699	0.0000	6.9×10^{4}
3	-2937	856	0.0001	2.5×10^{4}
4	-1616	1013	0.0035	194
5	-845	1120	0.0322	23
Values at 240 Hours				
1	12495	592	0.0000	1.2×10^{7}
2	4837	699	0.0001	7.7×10^{6}
3	1716	856	0.0011	1.9×10^{5}
4	736	1013	0.1142	1951
5	0	1120	1.0	-

Table 5. Load Case 4 Rupture Times

Values at 2 Hours				
Layer	Stress (psi)	Temperature (°C)	Life Fraction	Time to Rupture (Hr)
1	18710	595	0.0000	4.9×10^{5}
2	-2075	703	0.0000	8.4×10^{8}
3	-3801	862	0.0002	4243
4	-1854	1020	0.0060	96
5	-964	1128	0.0461	11
Values at 240 Hours				
1	7214	595	0.0000	6.3×10^{8}
2	-1695	703	0.0000	1.9×10^{9}
3	-822	862	0.0006	1.9×10^{6}
4	-295	1020	0.0366	2.6×10^{4}
5	-164	1128	0.3796	1159

An estimate of the vessel failure can be made by using the rupture time in layer 3 at 240 hours which was explained earlier in load cases 1 and 2. Thus, for load case 3 the time to failure would be 1.9×10^5 hours or about 21 years. Load case 4 has an estimated time to failure of the vessel of 1.9×10^6 hours or about 216 years. Obviously, the vessel will not fail due to creep rupture, because the pool will have cooled off in the time period.

7. Conclusions

The reactor vessels were assessed for failure after the molten core had deposited on the lower head of the vessel. Four different load combinations were analyzed. There were two different thermal loadings with steady state conditions based on nucleate and film boiling heat transfer from the vessel. Each thermal loading was analyzed for two pressure loadings of 75 psi (operating pressure) and 0 psi (assuming a pipe break). In all the analyses, the structure was assessed for two failure mechanisms of plastic instability and creep rupture of the vessel wall. The results of the analyses indicate that the vessel would survive for each loading case. Some slight damage to the vessel wall would occur near the centerline of the bottom head, but structural integrity would remain.

The finite element computer program, STRAW, was used to perform the above analyses. The addition of the viscoelastic/viscoplastic constitutive model and creep rupture algorithm now make it possible to assess the failure of reactor vessels to core melts or any other type of thermomechanical loadings.

Acknowledgments

Work supported by the U.S. Department of Energy, Office of New Production Reactors under Contract W-31-109-Eng-38.

References

Department of Defense, 1986, Aerospace Structural Metals Handbook, Code 1307, Materials and Ceramics Center, Battelle Columbus Laboratories, p. 37.

Dimelfi, R. J. and Kramer, J. M., 1980, "Modeling the Effects of Fast-Neutron Irradiation on the Subsequent Mechanical Behaviour of Type 316 Stainless Steel," Journal of Nuclear Materials, Vol. 89, pp. 338-346.

Kulak, R. F., Belytschko, T. B., Kennedy, J. M., and Schoeberle, D. F., 1978, "Finite Element Formulation for Thermal Stress Analysis of Thin Reactor Structures," Nuclear Engineering and Design, Vol. 49, pp. 39-50.

Larson, F. R. and Miller, J., 1952, "A Time-Temperature Relationship for Rupture and Creep Stresses," Transactions of the ASME, Vol. 74, pp. 765-775.

Schoeberle, D. F., Kennedy, J. M., and Belytschko, T. B., 1974, "Implicit Temporal Integration for Long-Duration Accidents in a Structural Response Code-STRAW," ANL-8136, Argonne National Laboratory, Argonne, Ill.

Schreyer, H. L., Kennedy, J. M., and Schoeberle, D. F., 1983, "Thermoviscoplastic Analysis of First Walls Subjected to Fusion Power Transients," Journal of Pressure Vessel Technology, Vol. 105, pp. 42-51.

List of Figures

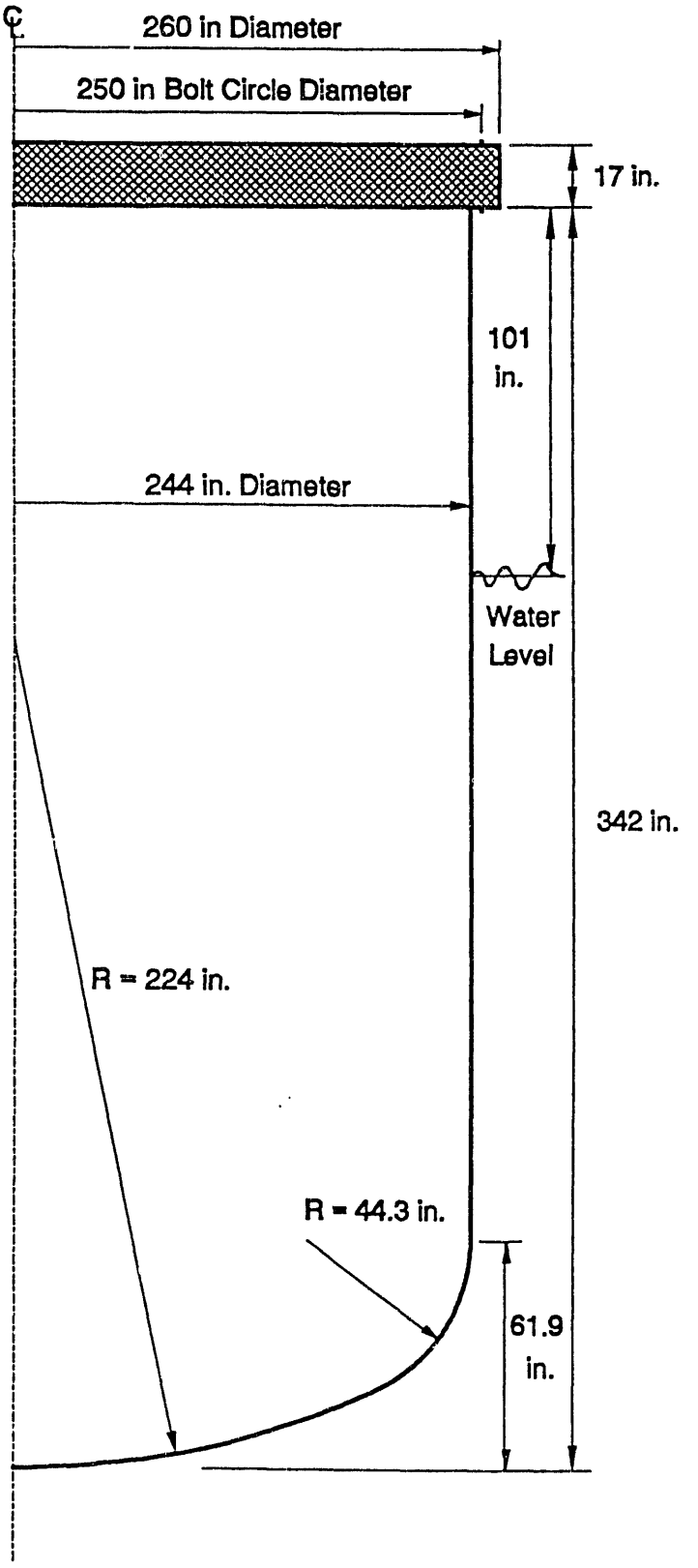
℄
260 in Diameter
250 in Bolt Circle Diameter
17 in.
101
in.
244 in. Diameter
Water
Level
342 in.
R = 224 in.
R = 44.3 in.
61.9
in.

Fig. 1

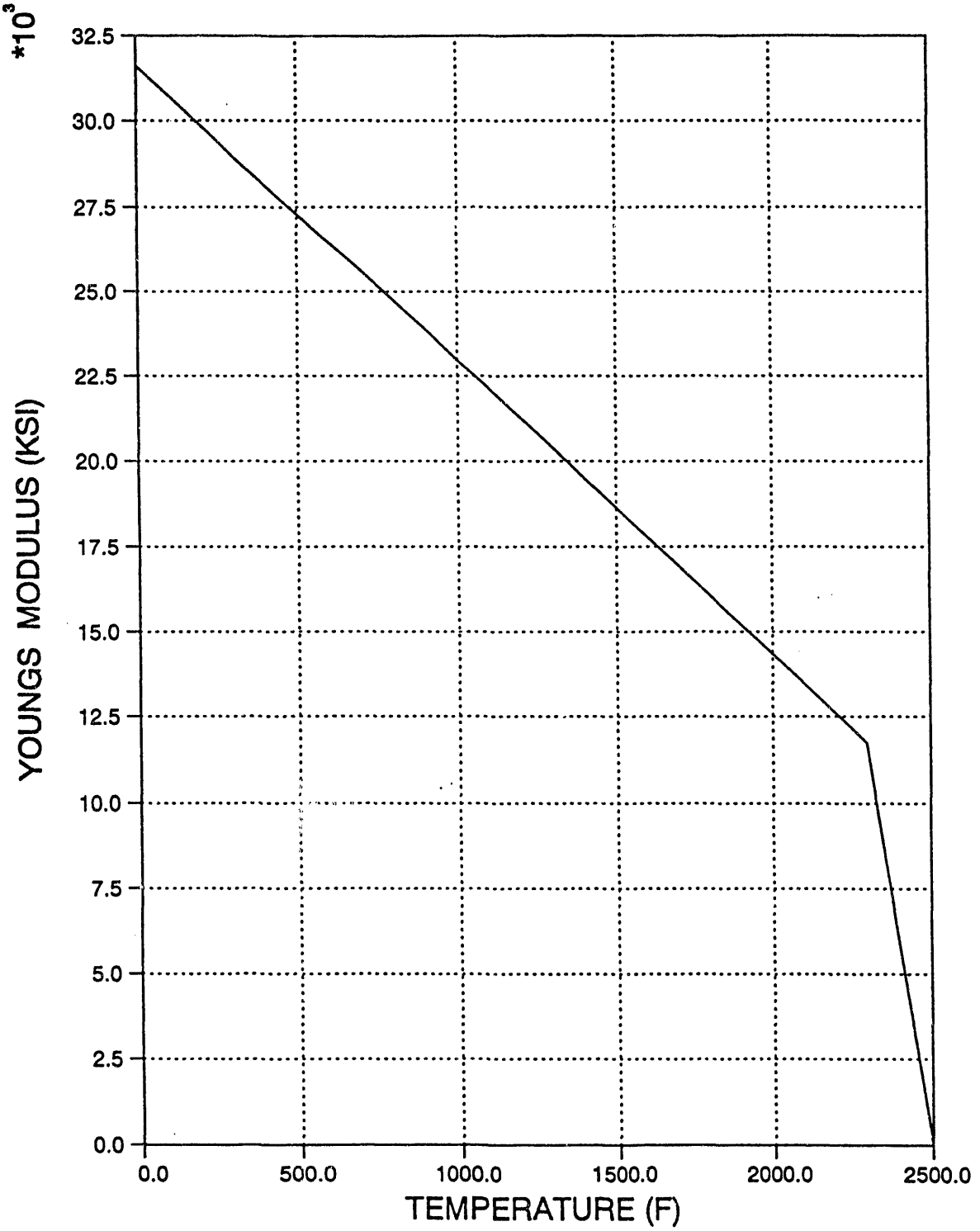
*10^3
32.5
30.0
27.5
25.0
22.5
20.0
17.5
15.0
12.5
10.0
7.5
5.0
2.5
0.0
YOUNGS MODULUS (KSI)
0.0
500.0
1000.0
1500.0
2000.0
2500.0
TEMPERATURE (F)

Fig. 2

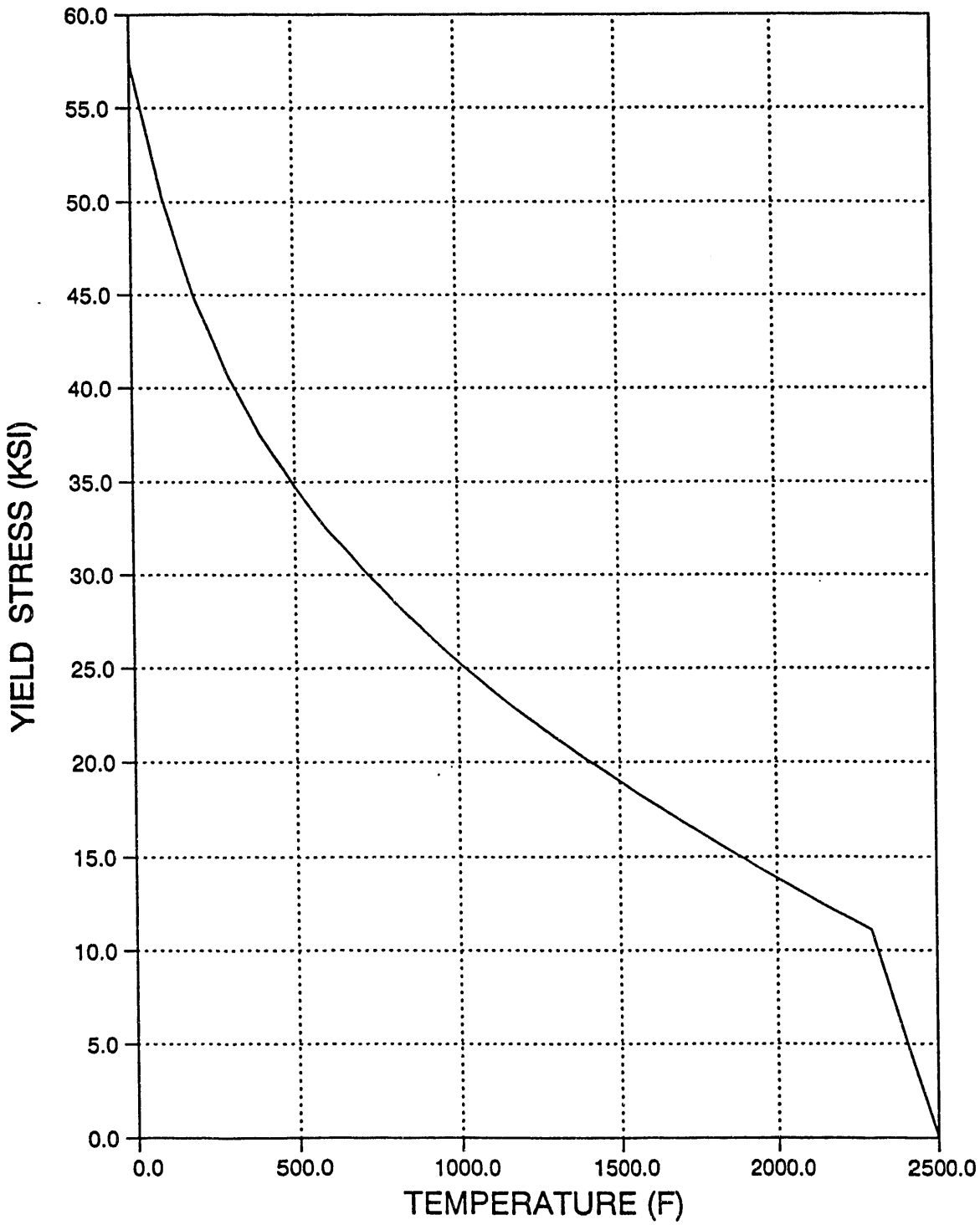
60.0
55.0
50.0
45.0
40.0
35.0
30.0
25.0
20.0
15.0
10.0
5.0
0.0
YIELD STRESS (KSI)
0.0
500.0
1000.0
1500.0
2000.0
2500.0
TEMPERATURE (F)

Fig. 3

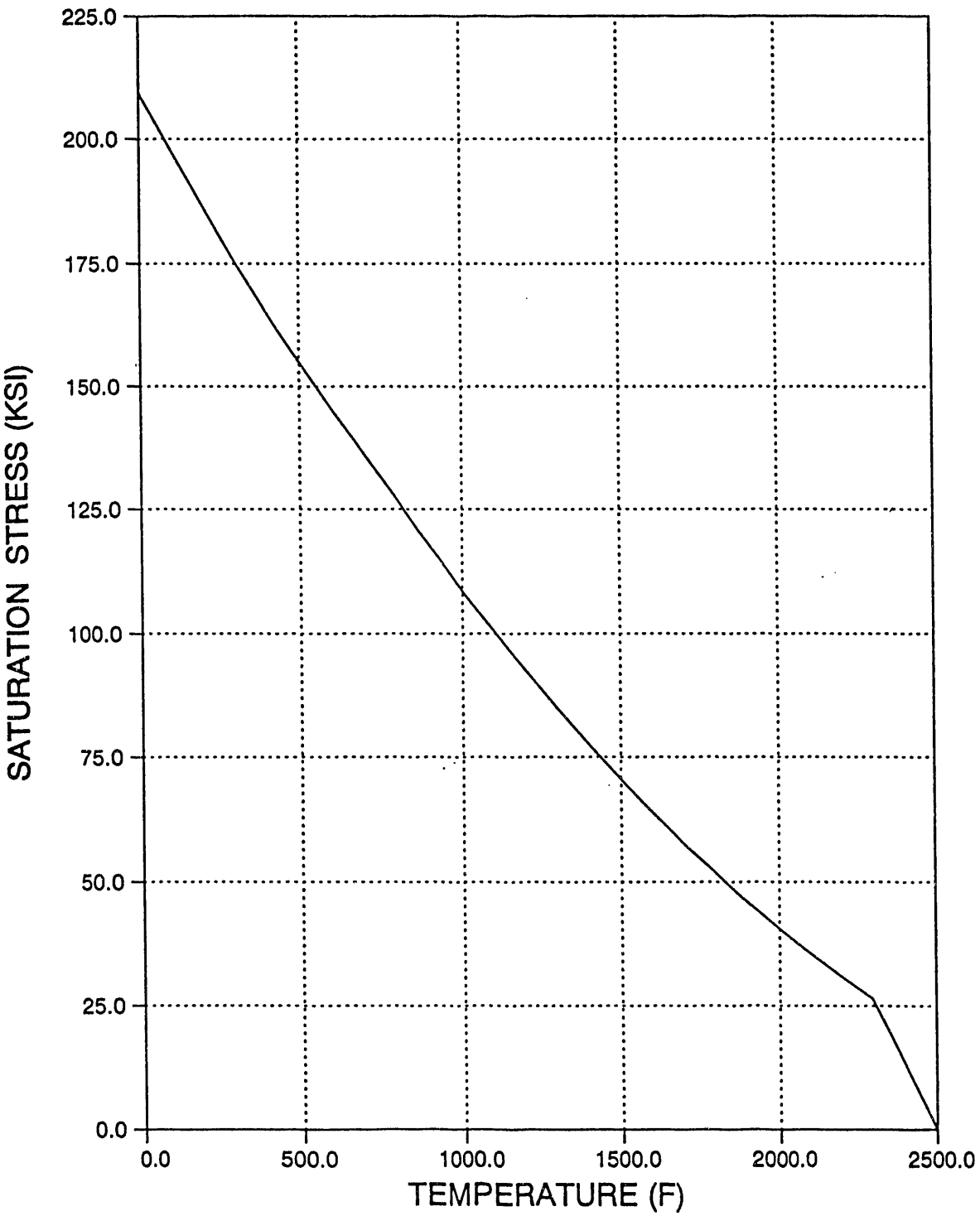
225.0
200.0
175.0
150.0
125.0
100.0
75.0
50.0
25.0
0.0
SATURATION STRESS (KSI)
0.0
500.0
1000.0
1500.0
2000.0
2500.0
TEMPERATURE (F)

Fig. 4

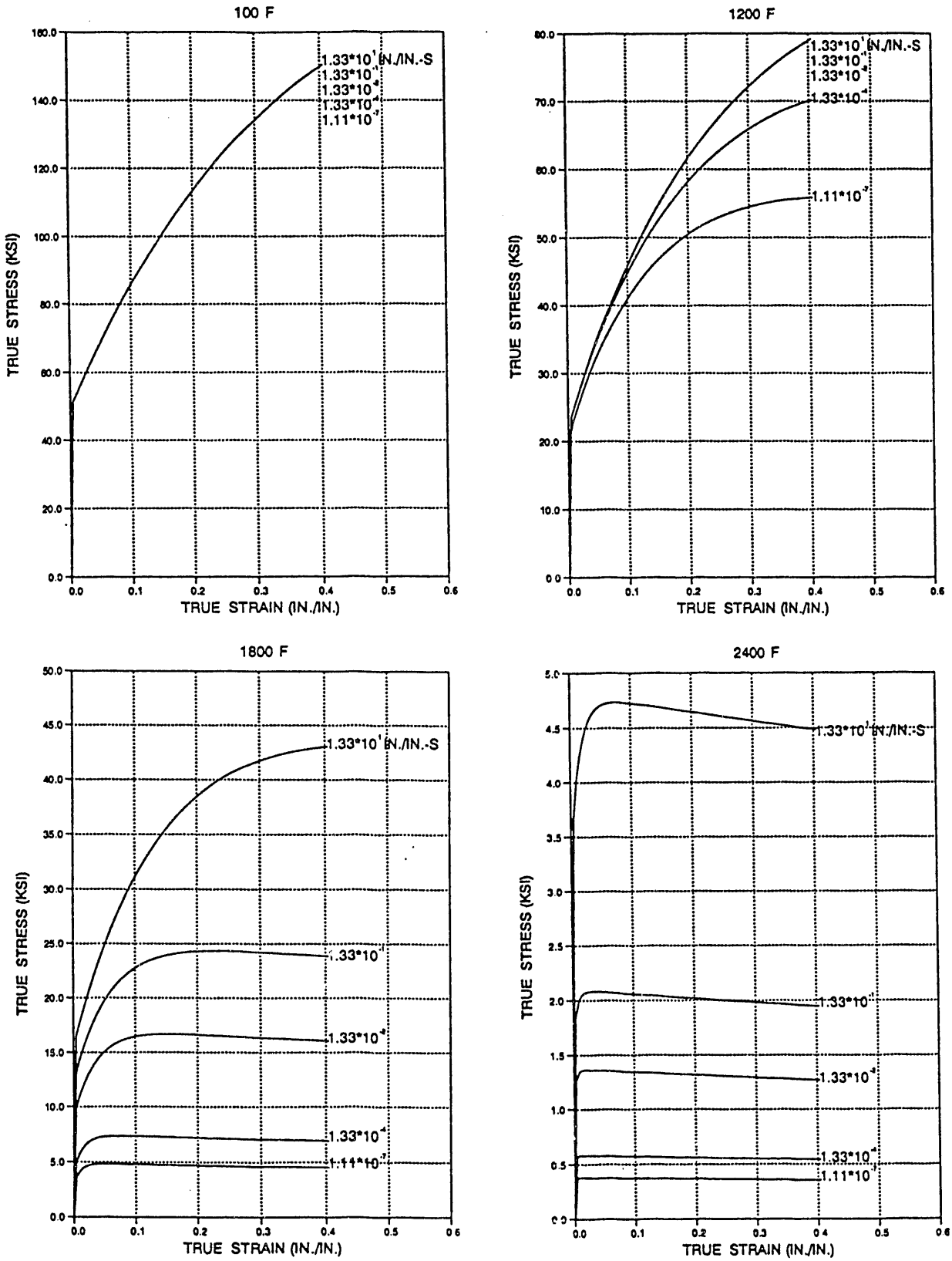
100 F
TRUE STRESS (KSI)
TRUE STRAIN (IN./IN.)
1.33*10^1 IN./IN.-S
1.33*10^-1
1.33*10^-2
1.33*10^-4
1.11*10^-7
1200 F
TRUE STRESS (KSI)
TRUE STRAIN (IN./IN.)
1.33*10^1 IN./IN.-S
1.33*10^-1
1.33*10^-2
1.33*10^-4
1.11*10^-7
1800 F
TRUE STRESS (KSI)
TRUE STRAIN (IN./IN.)
1.33*10^1 IN./IN.-S
1.33*10^-1
1.33*10^-2
1.33*10^-4
1.11*10^-7
2400 F
TRUE STRESS (KSI)
TRUE STRAIN (IN./IN.)
1.33*10^1 IN./IN.-S
1.33*10^-1
1.33*10^-2
1.33*10^-4
1.33*10^-4
1.11*10^-7

Fig. 5

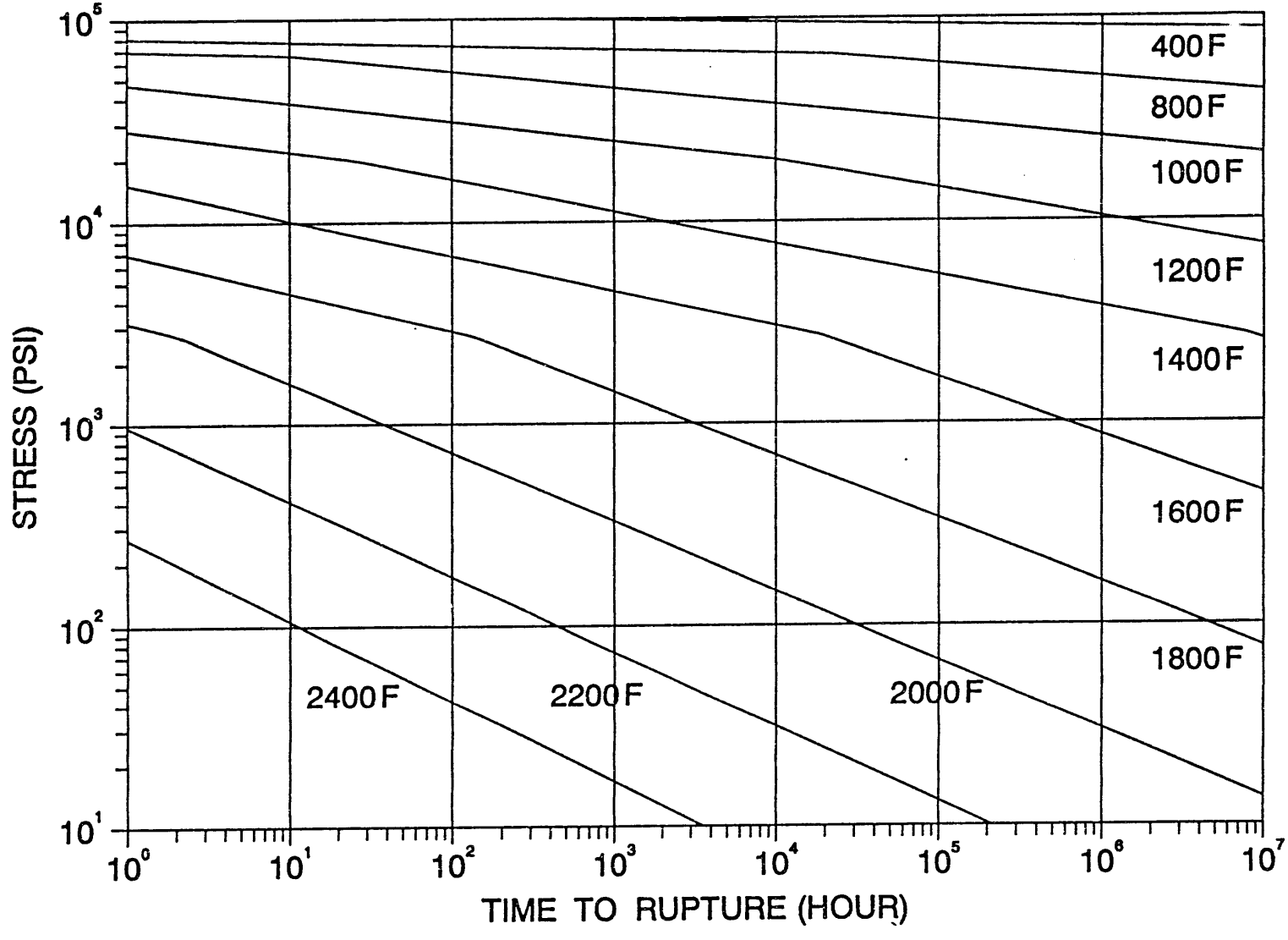
STRESS (PSI)
10^5
10^4
10^3
10^2
10^1
400F
800F
1000F
1200F
1400F
1600F
1800F
2000F
2200F
2400F
10^0
10^1
10^2
10^3
10^4
10^5
10^6
10^7
TIME TO RUPTURE (HOUR)

Fig. 6

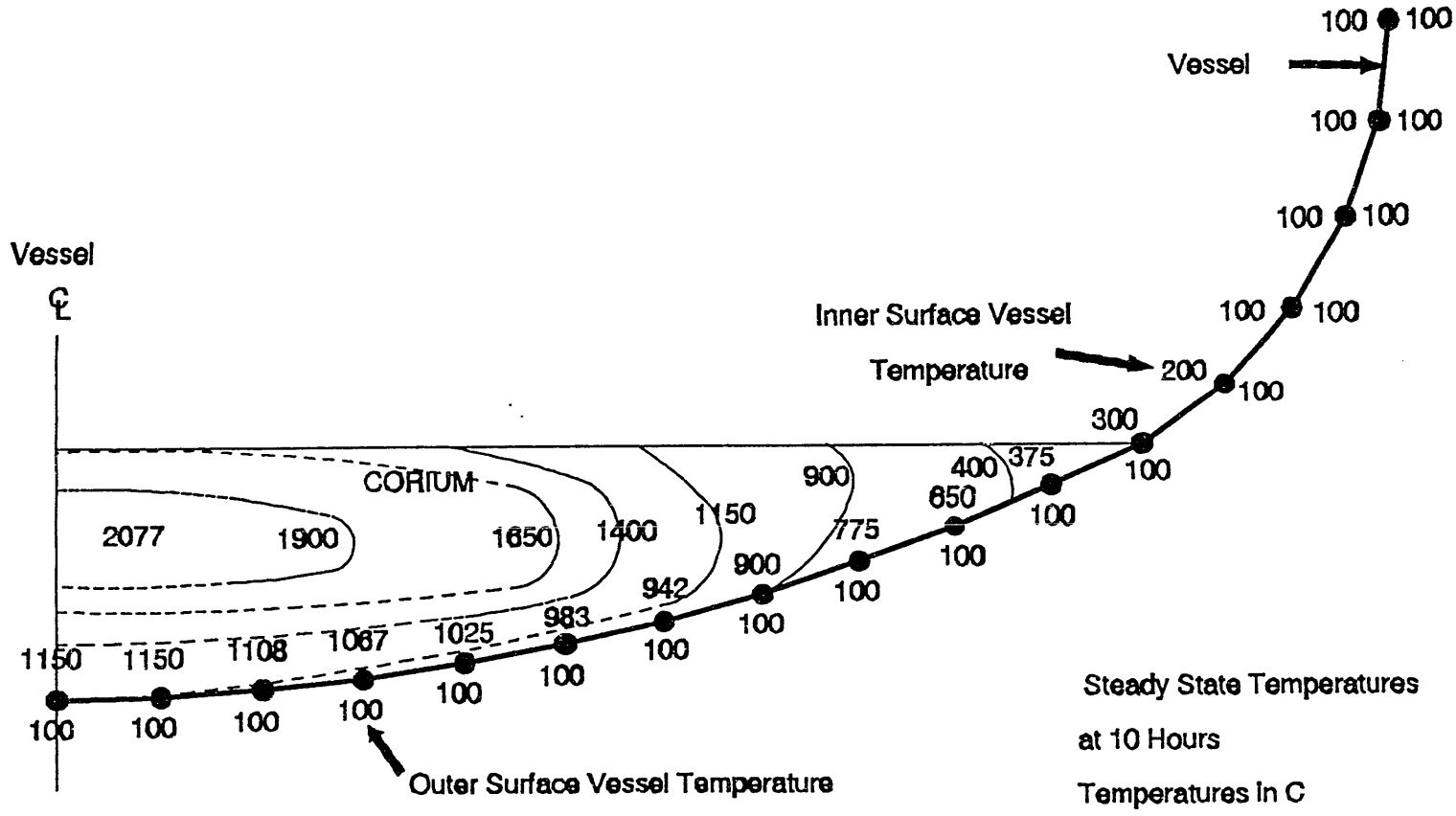
Vessel
℄
CORIUM
2077
1900
1650
1400
1150
900
775
650
400
375
300
200
100
942
983
1025
1067
1108
1150
1150
Inner Surface Vessel
Temperature
Vessel
Outer Surface Vessel Temperature
Steady State Temperatures
at 10 Hours
Temperatures In C

Fig. 7

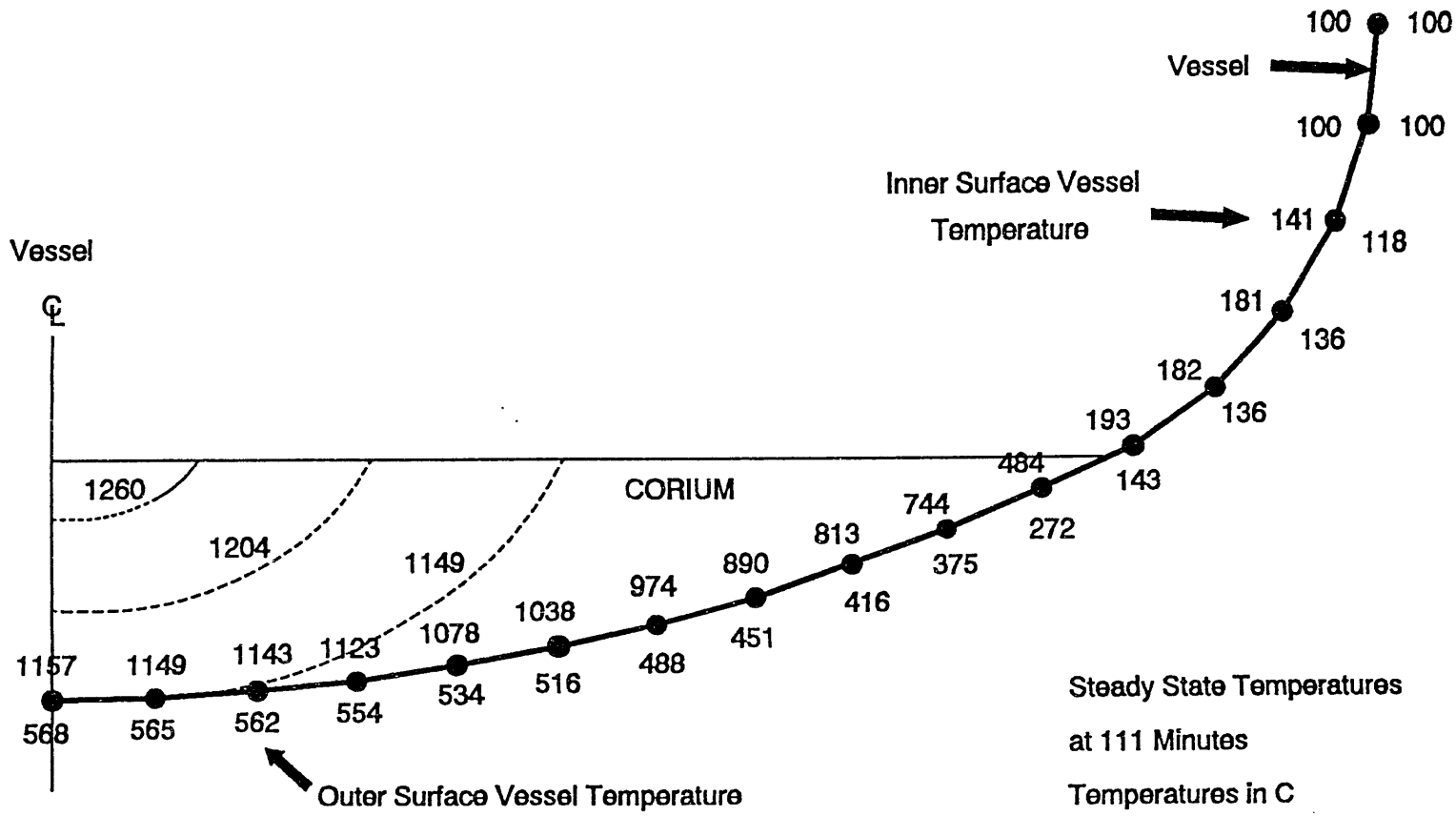
Vessel
Inner Surface Vessel Temperature
Vessel
CORIUM
1260
1204
1149
100
100
100
100
141
118
181
136
182
136
193
143
484
272
744
375
813
416
890
451
974
488
1038
516
1078
534
1157
1149
1143
1123
568
565
562
554
Outer Surface Vessel Temperature
Steady State Temperatures
at 111 Minutes
Temperatures in C

Fig. 8

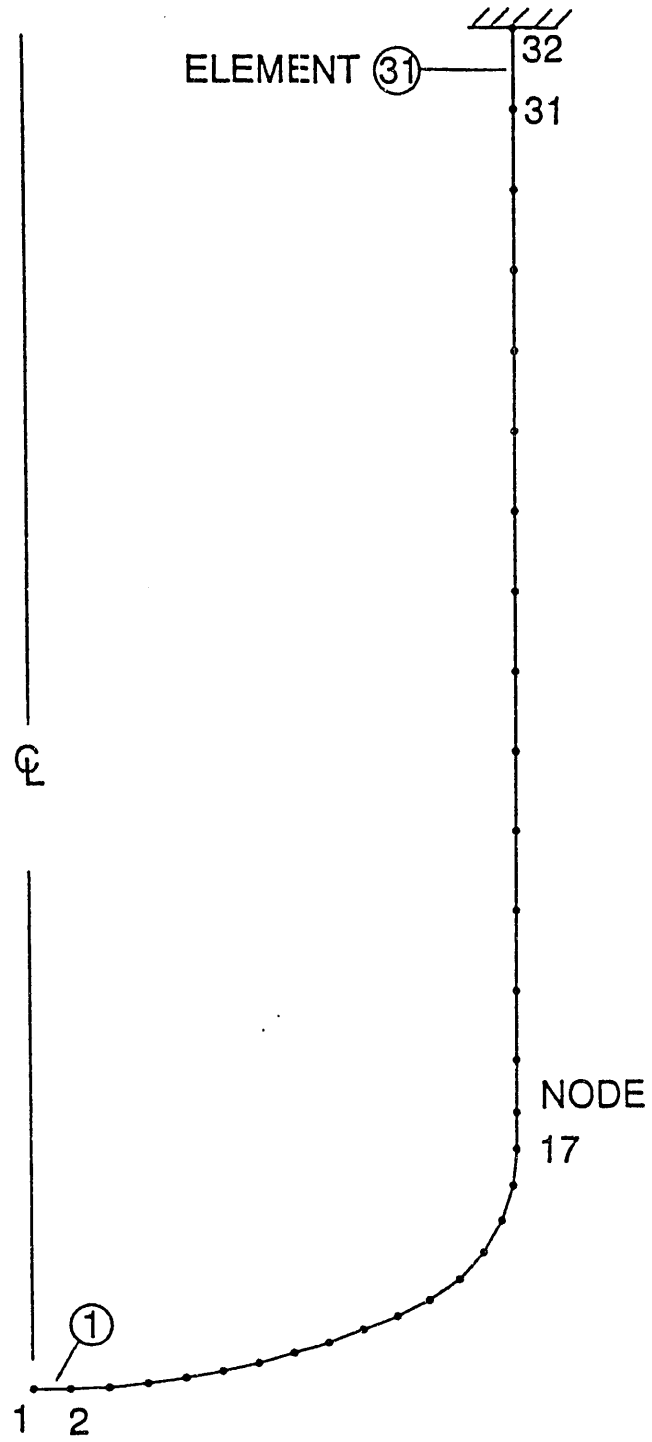

Fig. 9

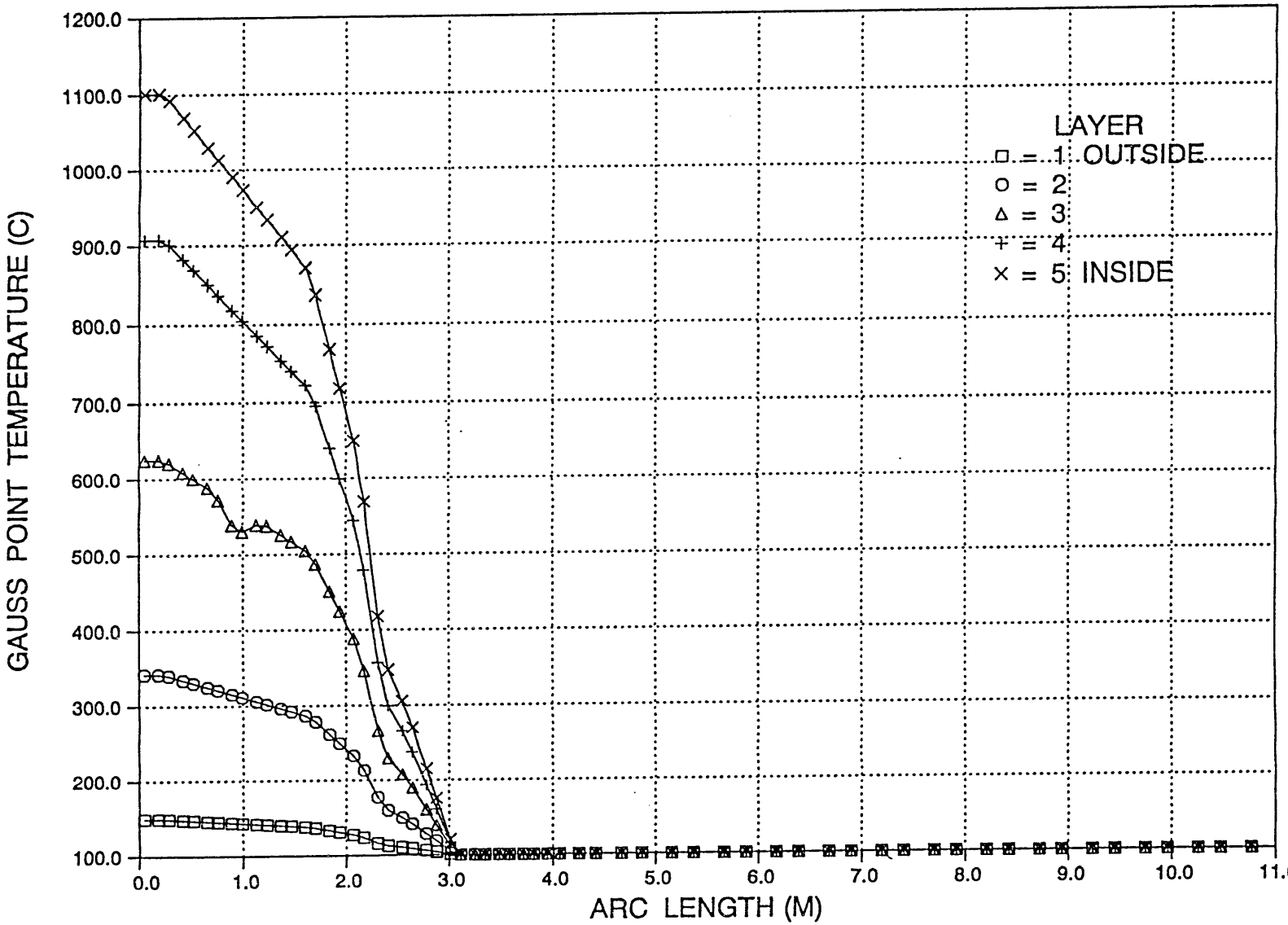
GAUSS POINT TEMPERATURE (C)
1200.0
1100.0
1000.0
900.0
800.0
700.0
600.0
500.0
400.0
300.0
200.0
100.0
0.0
1.0
2.0
3.0
4.0
5.0
6.0
7.0
8.0
9.0
10.0
11.0
ARC LENGTH (M)
LAYER
□ = 1 OUTSIDE
○ = 2
△ = 3
+ = 4
× = 5 INSIDE

Fig. 10

MESH PLOT FOR 75 PSI INTERNAL PRESSURE
DISPLACEMENT MAGNIFICATION = 10

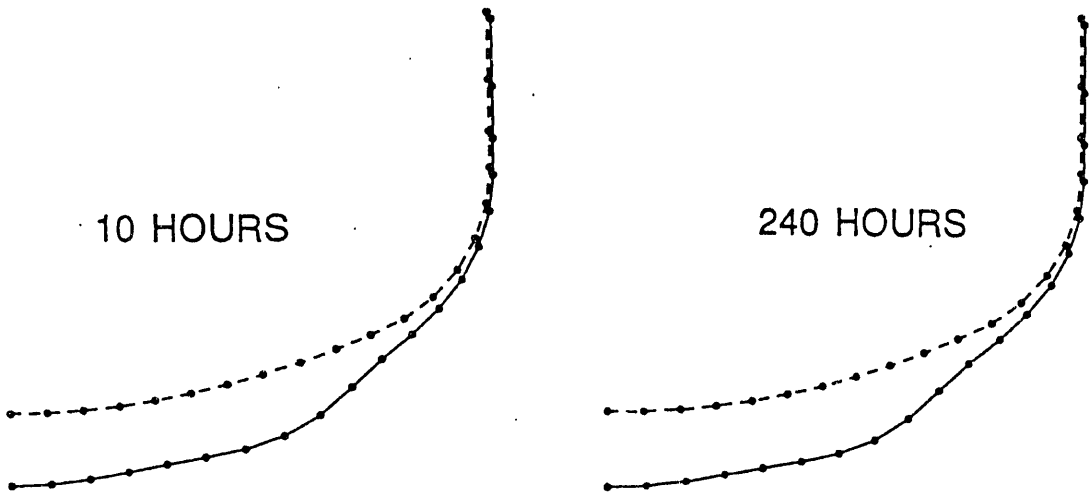

MESH PLOT FOR 0 PSI INTERNAL PRESSURE
DISPLACEMENT MAGNIFICATION = 10

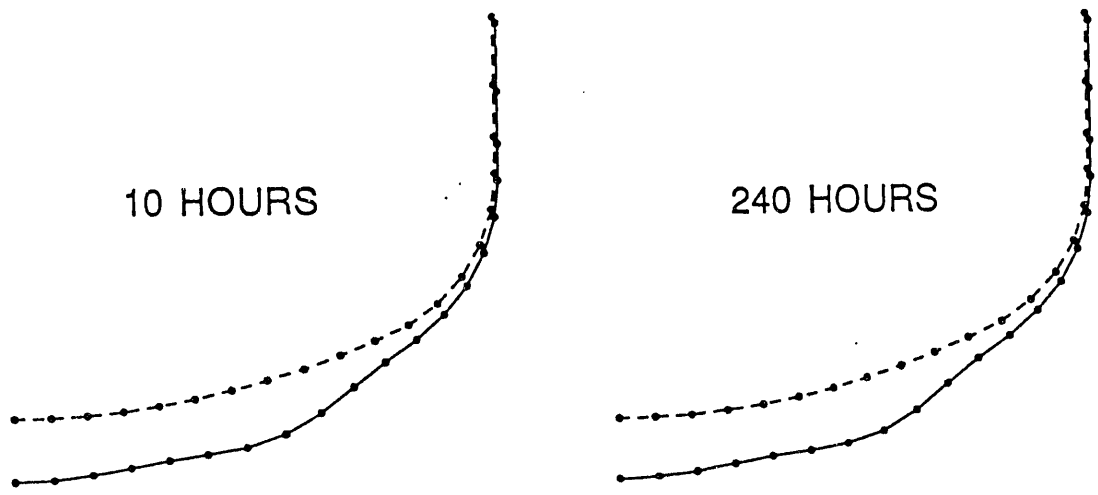

Fig. 11

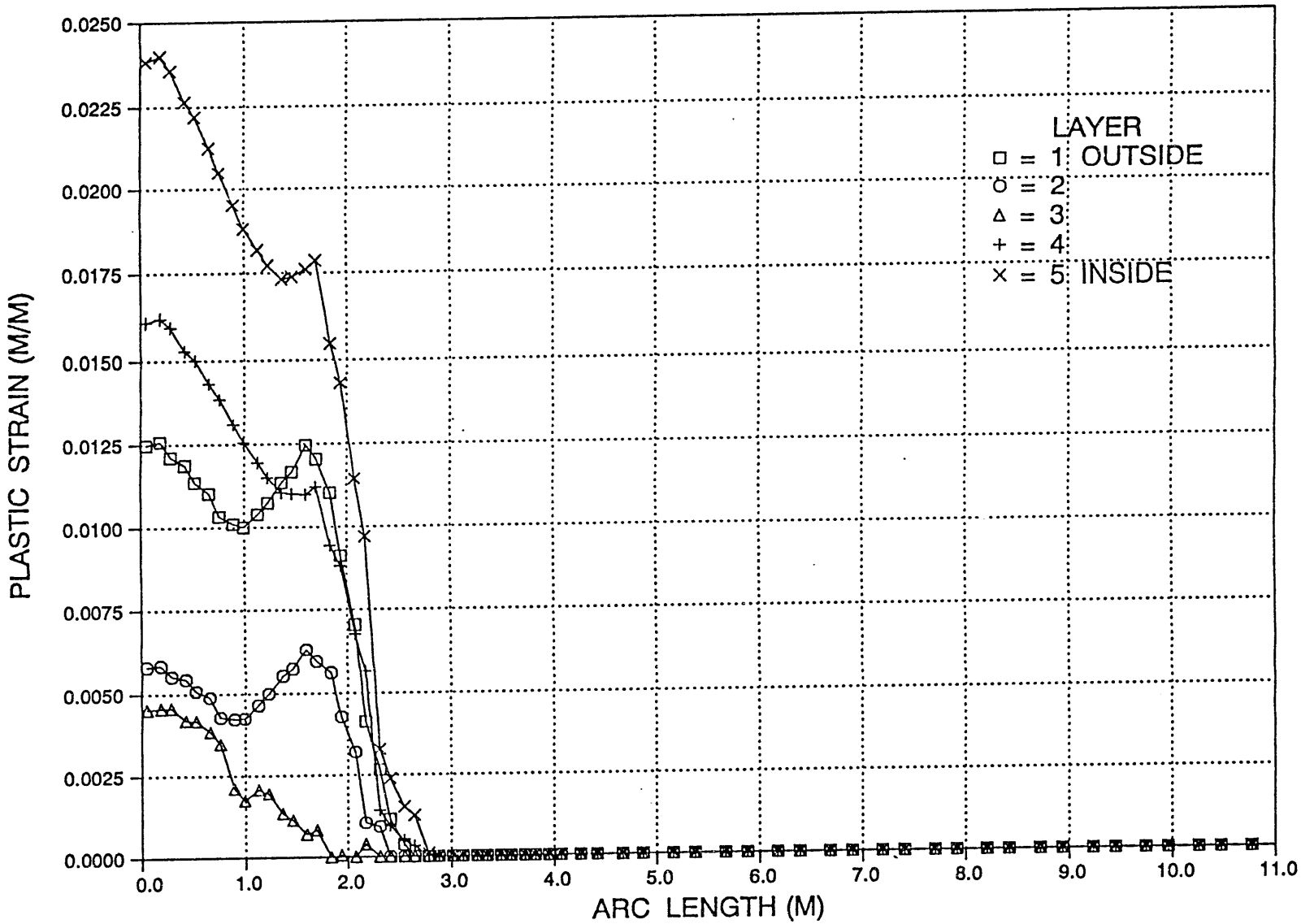
PLASTIC STRAIN (M/M)
0.0250
0.0225
0.0200
0.0175
0.0150
0.0125
0.0100
0.0075
0.0050
0.0025
0.0000
0.0
1.0
2.0
3.0
4.0
5.0
6.0
7.0
8.0
9.0
10.0
11.0
ARC LENGTH (M)
LAYER
□ = 1 OUTSIDE
○ = 2
△ = 3
+ = 4
× = 5 INSIDE

Fig. 12

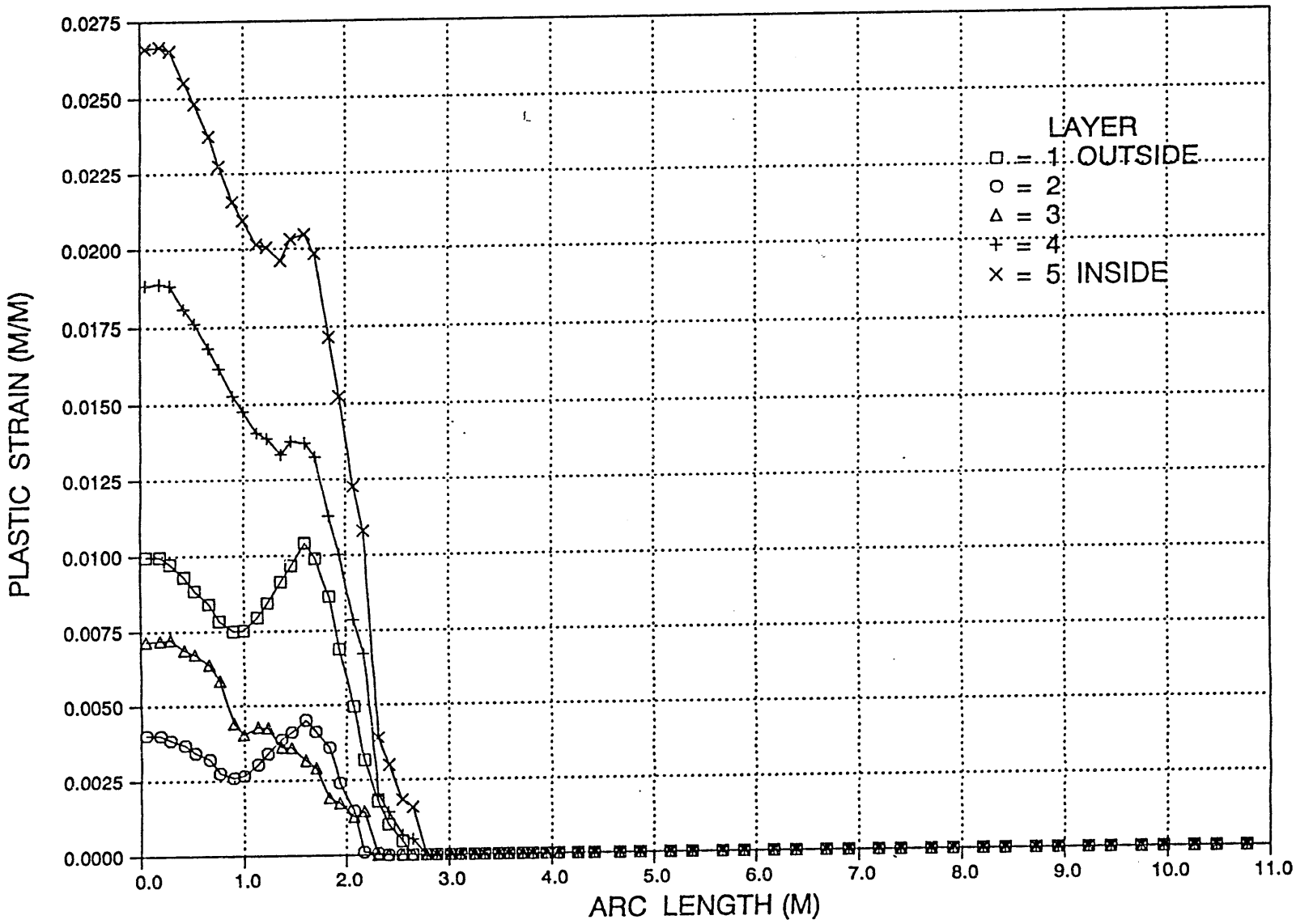
PLASTIC STRAIN (M/M)
0.0275
0.0250
0.0225
0.0200
0.0175
0.0150
0.0125
0.0100
0.0075
0.0050
0.0025
0.0000
0.0
1.0
2.0
3.0
4.0
5.0
6.0
7.0
8.0
9.0
10.0
11.0
ARC LENGTH (M)
LAYER
□ = 1 OUTSIDE
○ = 2
△ = 3
+ = 4
× = 5 INSIDE

Fig. 13

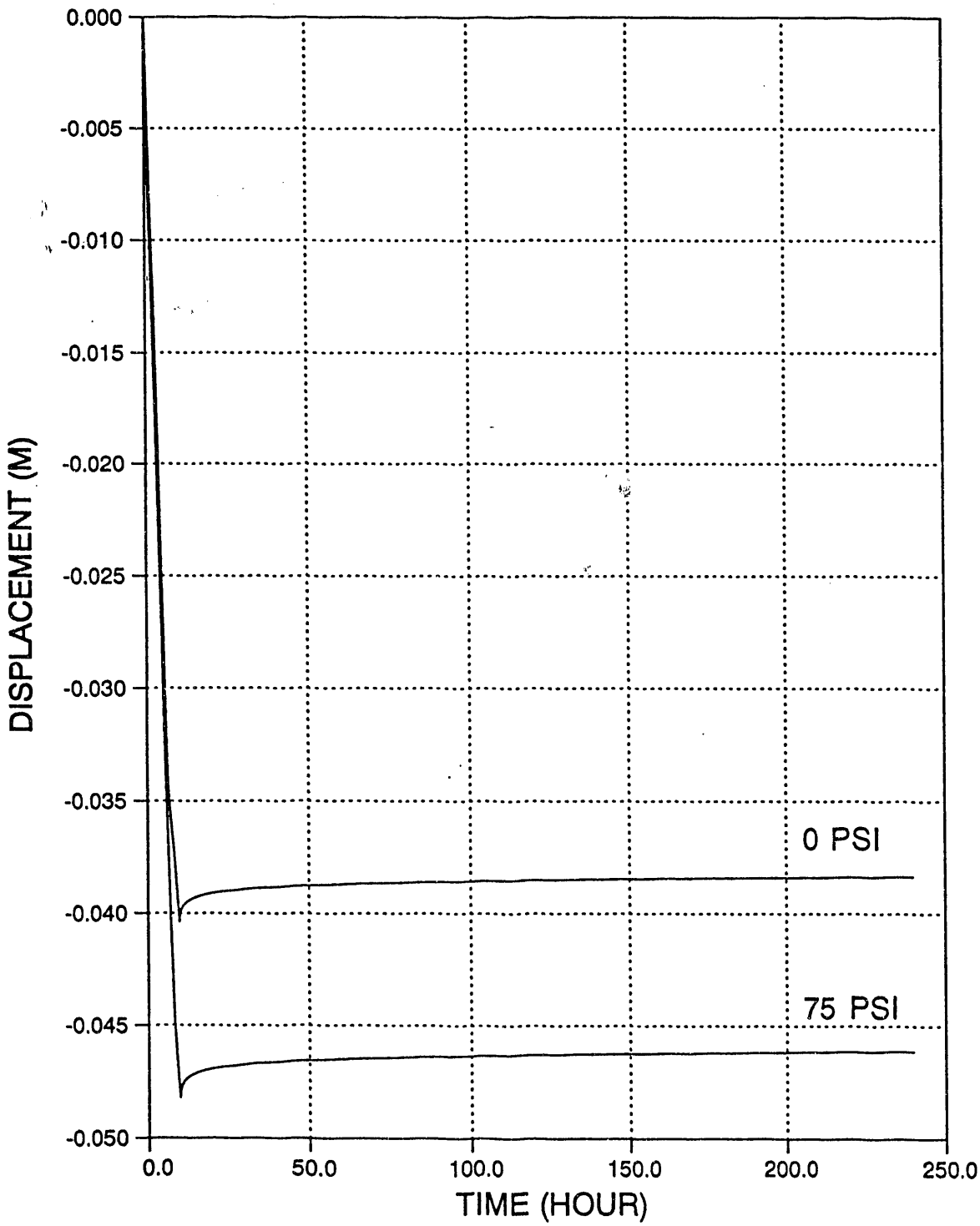
0.000
-0.005
-0.010
-0.015
-0.020
-0.025
-0.030
-0.035
-0.040
-0.045
-0.050
DISPLACEMENT (M)
0 PSI
75 PSI
0.0
50.0
100.0
150.0
200.0
250.0
TIME (HOUR)

Fig. 14

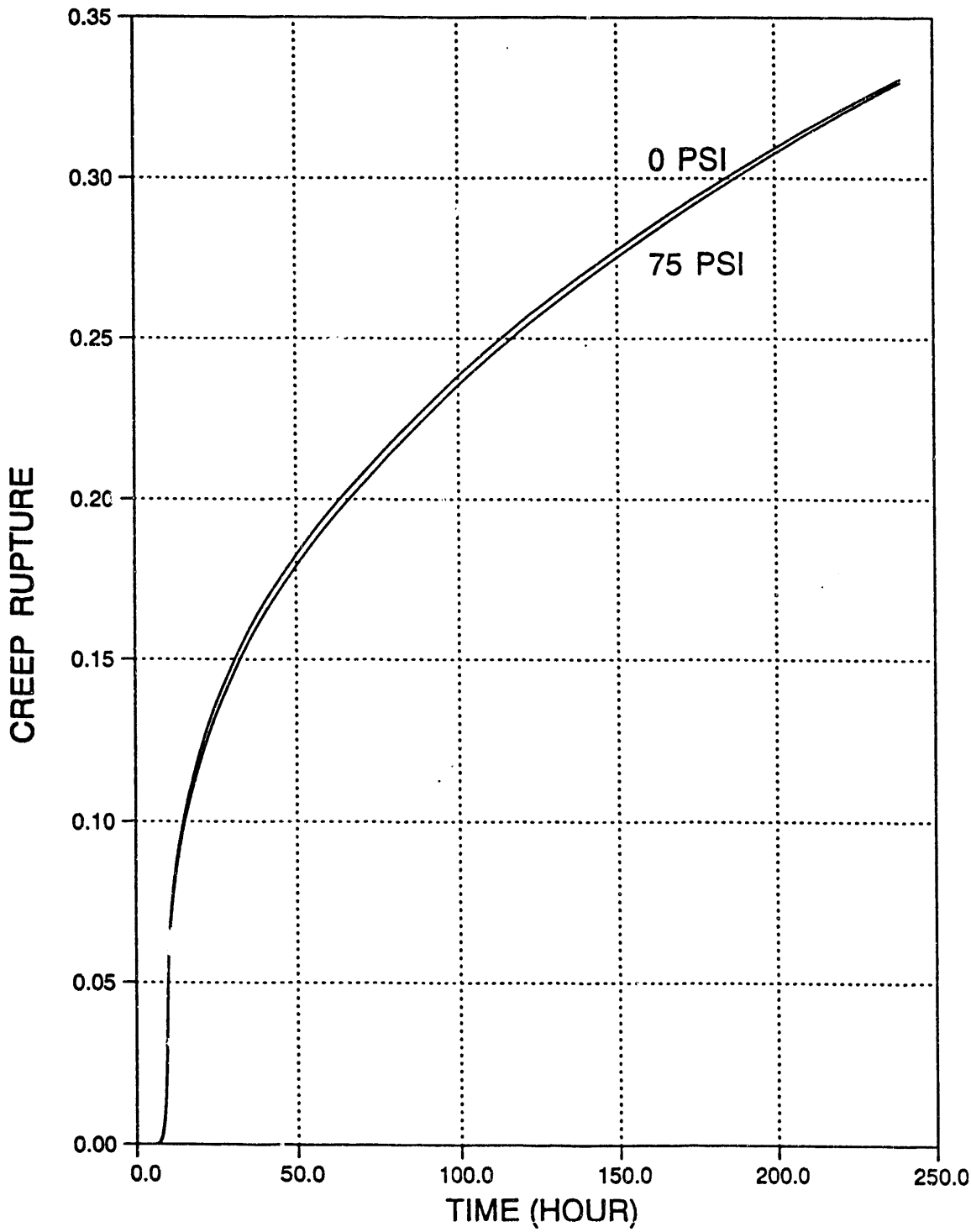
0.35
0.30
0.25
0.20
0.15
0.10
0.05
0.00
CREEP RUPTURE
0 PSI
75 PSI
0.0
50.0
100.0
150.0
200.0
250.0
TIME (HOUR)

Fig. 15

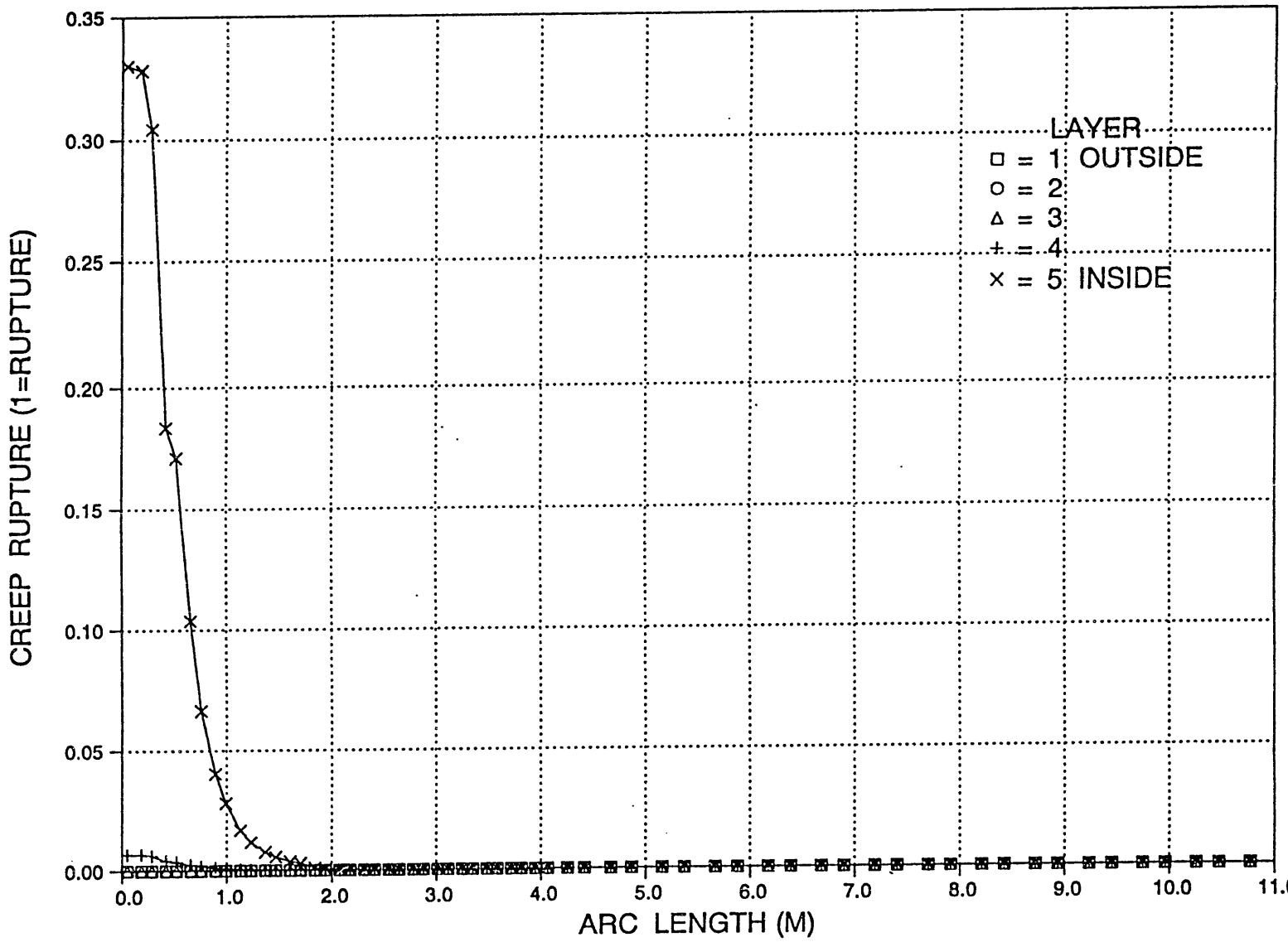
CREEP RUPTURE (1=RUPTURE)
0.35
0.30
0.25
0.20
0.15
0.10
0.05
0.00
0.0
1.0
2.0
3.0
4.0
5.0
6.0
7.0
8.0
9.0
10.0
11.0
ARC LENGTH (M)
LAYER
□ = 1 OUTSIDE
○ = 2
△ = 3
+ = 4
× = 5 INSIDE

Fig. 16

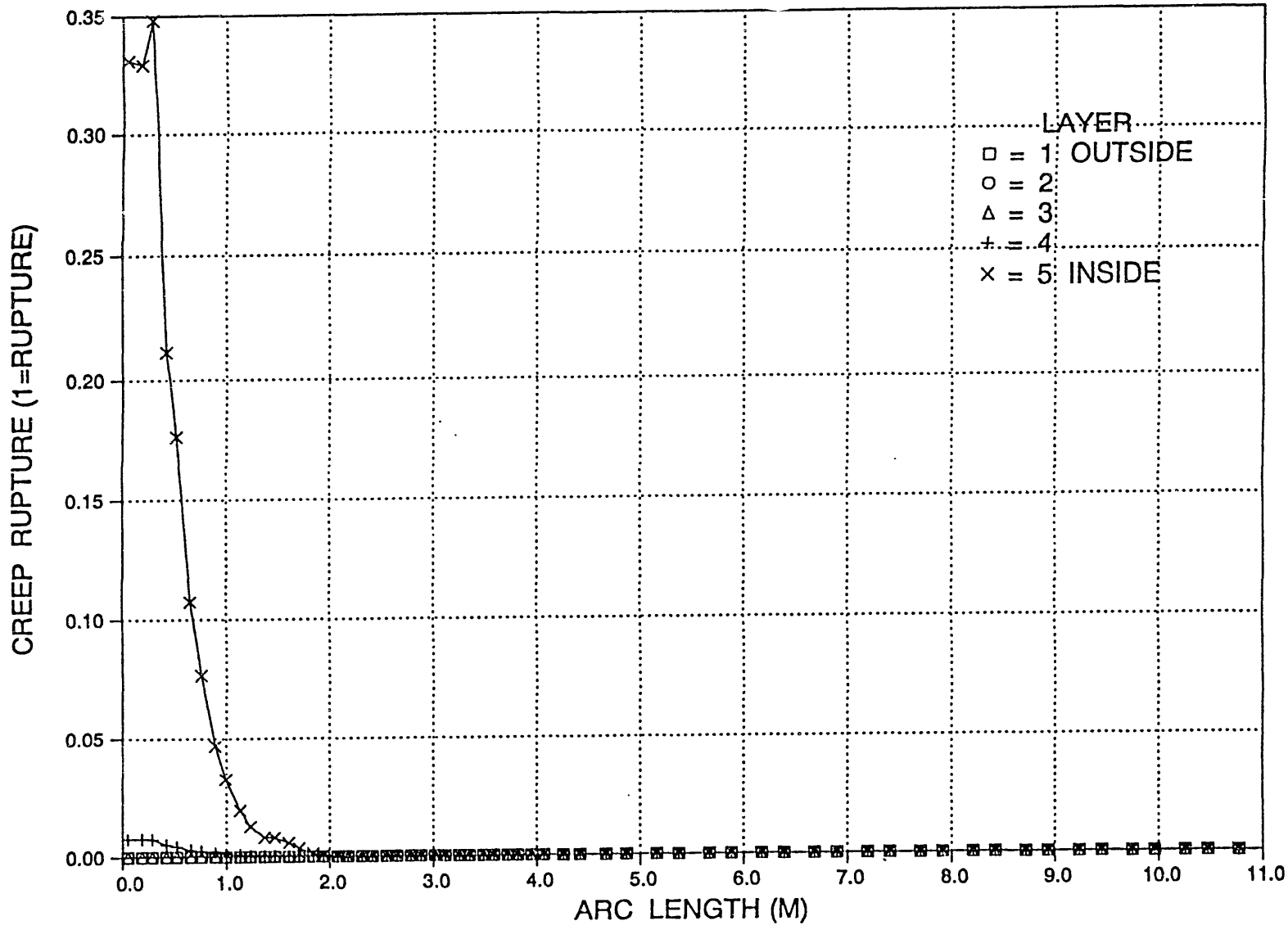
CREEP RUPTURE (1=RUPTURE)
0.35
0.30
0.25
0.20
0.15
0.10
0.05
0.00
0.0
1.0
2.0
3.0
4.0
5.0
6.0
7.0
8.0
9.0
10.0
11.0
ARC LENGTH (M)
LAYER
□ = 1 OUTSIDE
o = 2
Δ = 3
+ = 4
× = 5 INSIDE

Fig. 17

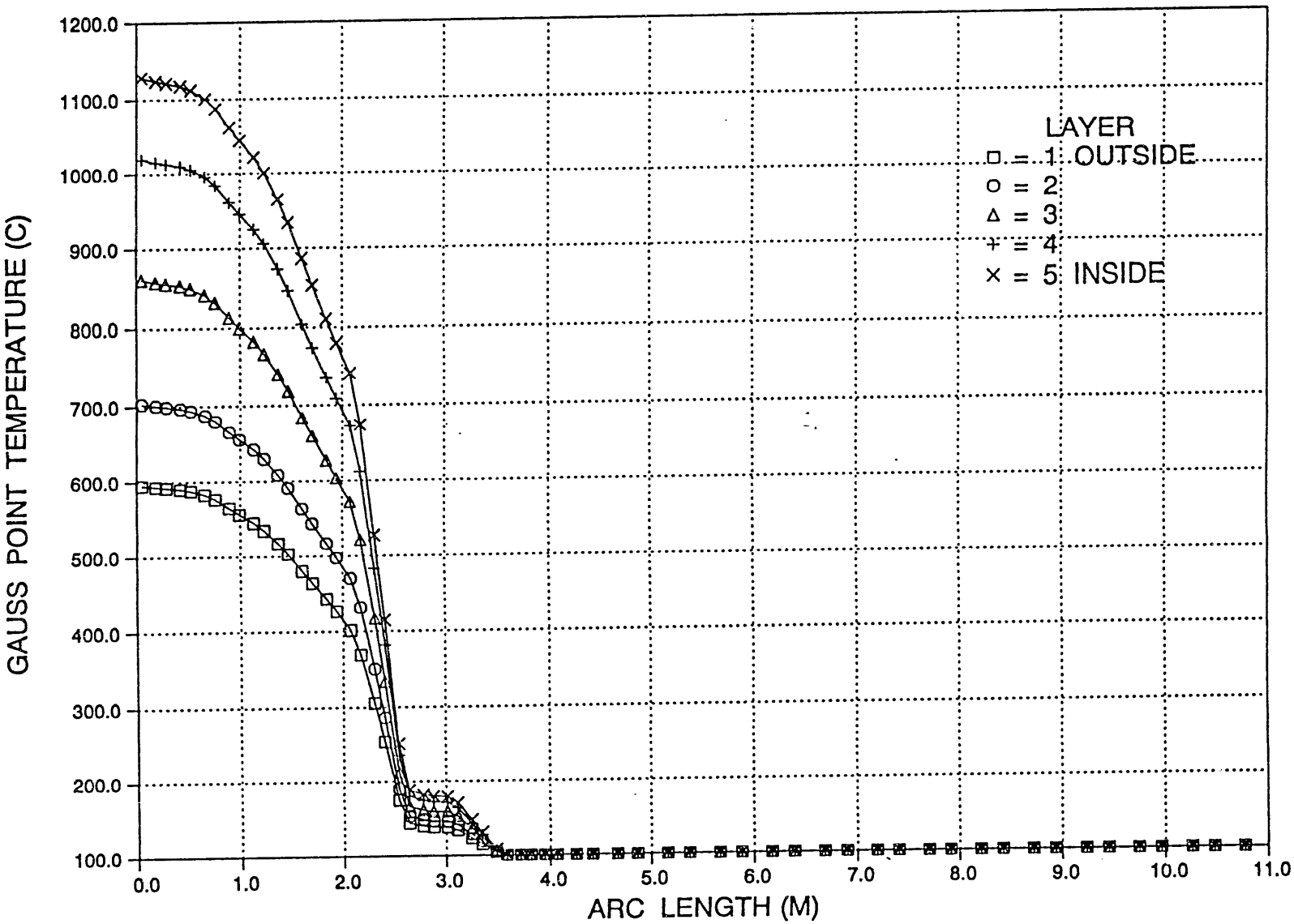
GAUSS POINT TEMPERATURE (C)
1200.0
1100.0
1000.0
900.0
800.0
700.0
600.0
500.0
400.0
300.0
200.0
100.0
0.0
1.0
2.0
3.0
4.0
5.0
6.0
7.0
8.0
9.0
10.0
11.0
ARC LENGTH (M)
LAYER
□ = 1 OUTSIDE
○ = 2
△ = 3
+ = 4
× = 5 INSIDE

Fig. 18

MESH PLOT FOR 75 PSI INTERNAL PRESSURE
DISPLACEMENT MAGNIFICATION = 10

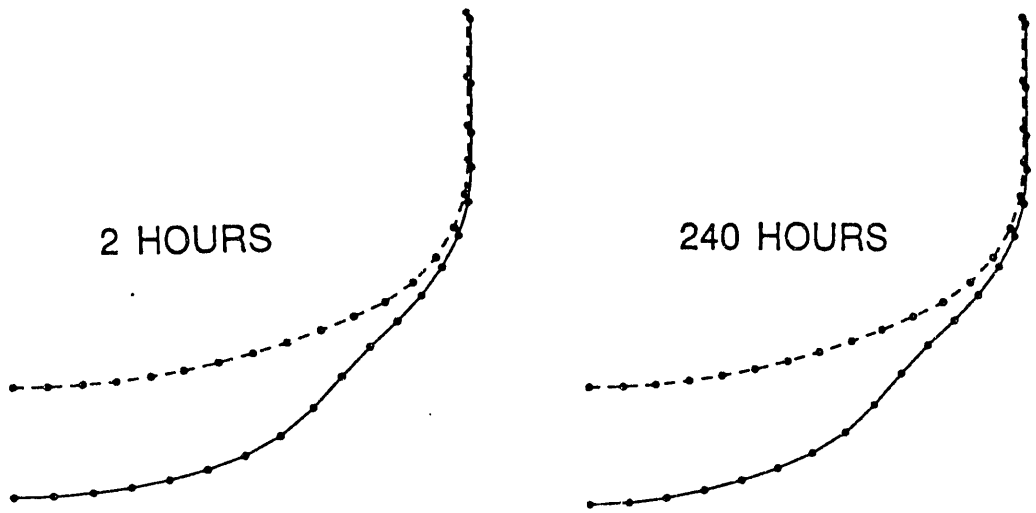

MESH PLOT FOR 0 PSI INTERNAL PRESSURE
DISPLACEMENT MAGNIFICATION = 10

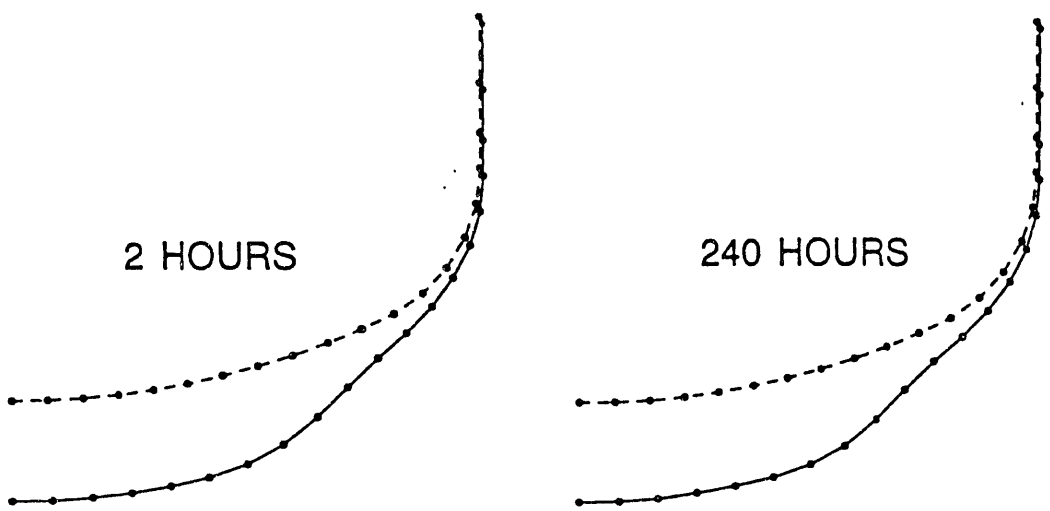

Fig. 19

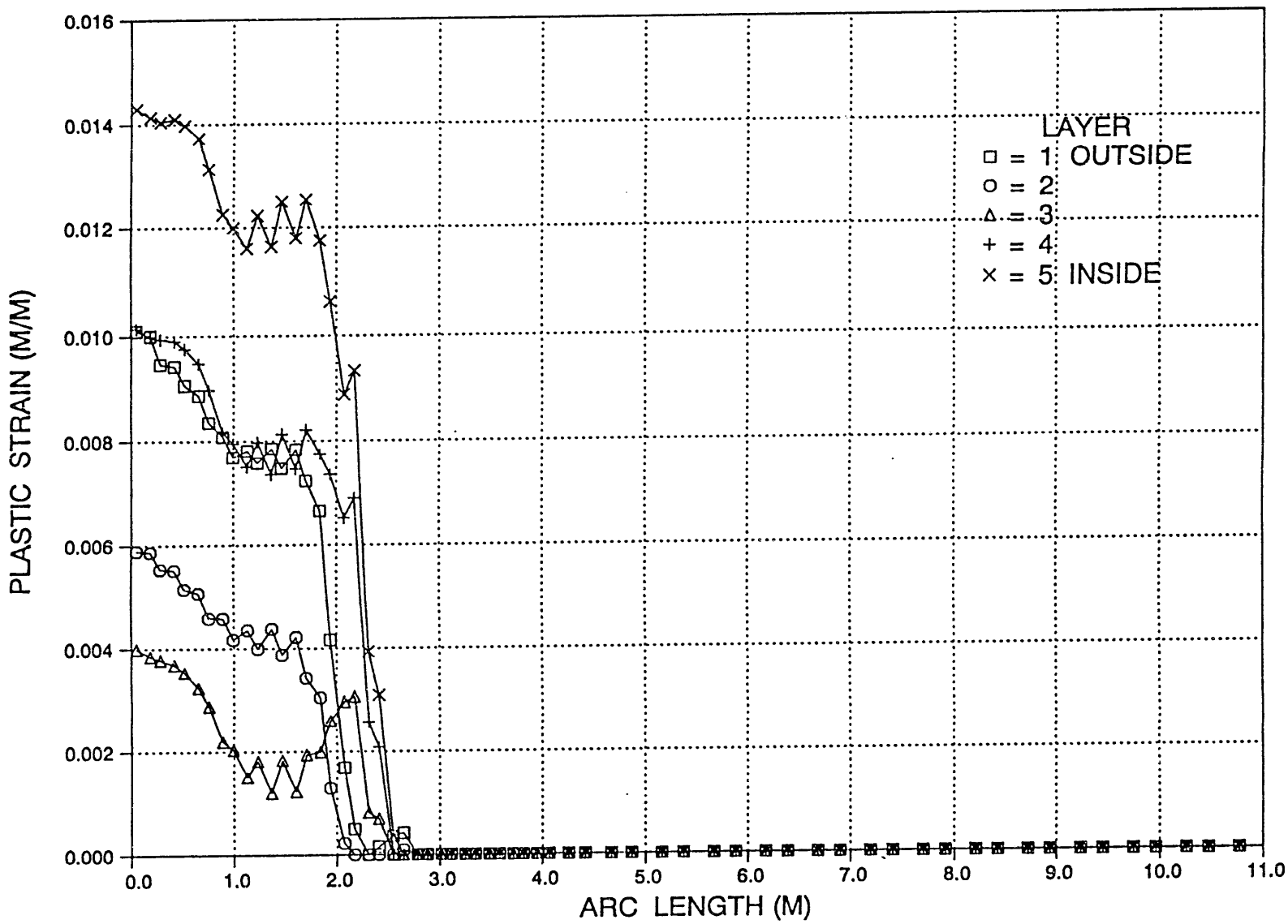
PLASTIC STRAIN (M/M)
0.016
0.014
0.012
0.010
0.008
0.006
0.004
0.002
0.000
0.0
1.0
2.0
3.0
4.0
5.0
6.0
7.0
8.0
9.0
10.0
11.0
ARC LENGTH (M)
LAYER
□ = 1 OUTSIDE
○ = 2
△ = 3
+ = 4
× = 5 INSIDE

Fig. 20

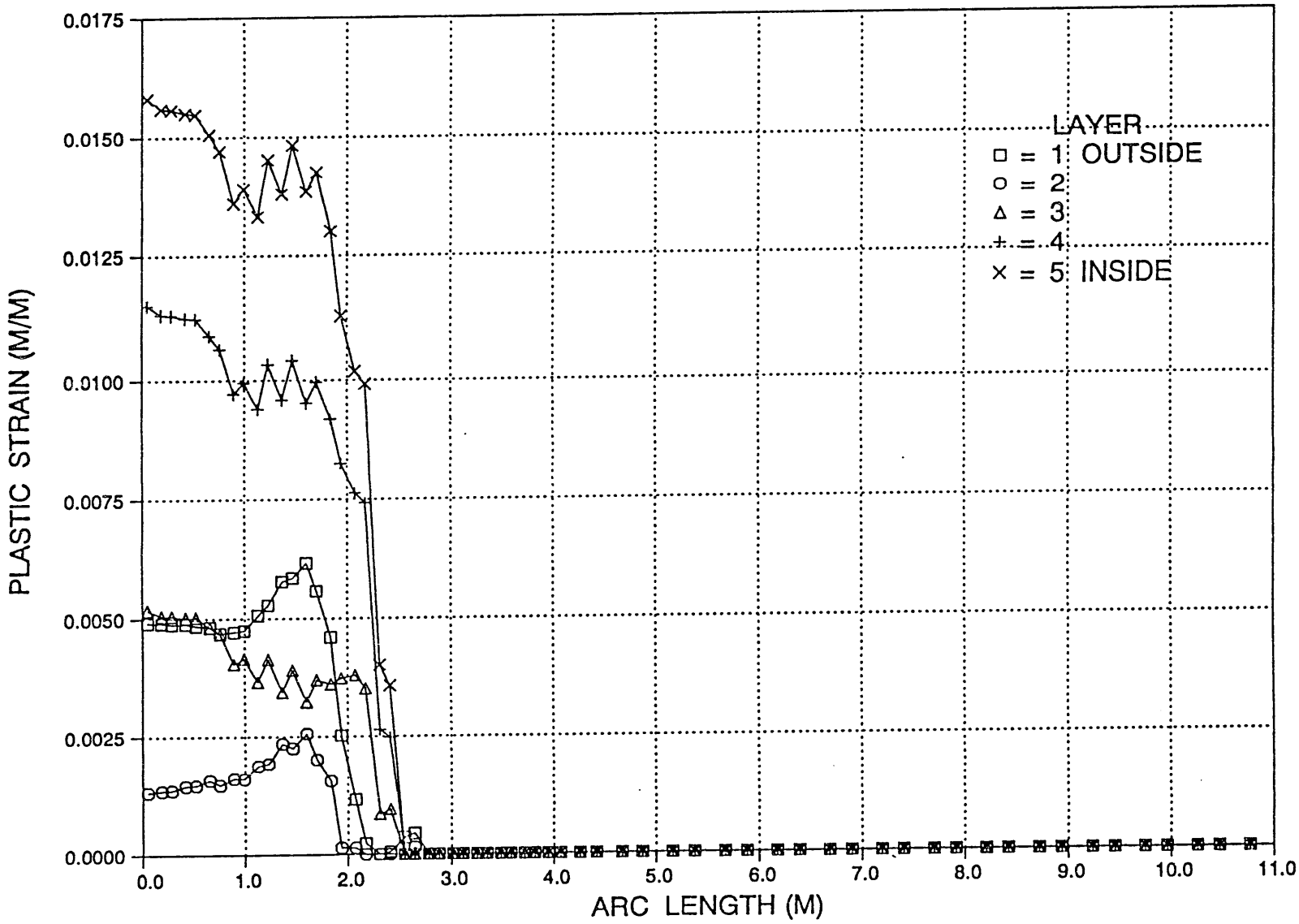
0.0175
0.0150
0.0125
0.0100
0.0075
0.0050
0.0025
0.0000
PLASTIC STRAIN (M/M)
0.0
1.0
2.0
3.0
4.0
5.0
6.0
7.0
8.0
9.0
10.0
11.0
ARC LENGTH (M)
LAYER
□ = 1 OUTSIDE
○ = 2
△ = 3
+ = 4
× = 5 INSIDE

Fig. 21

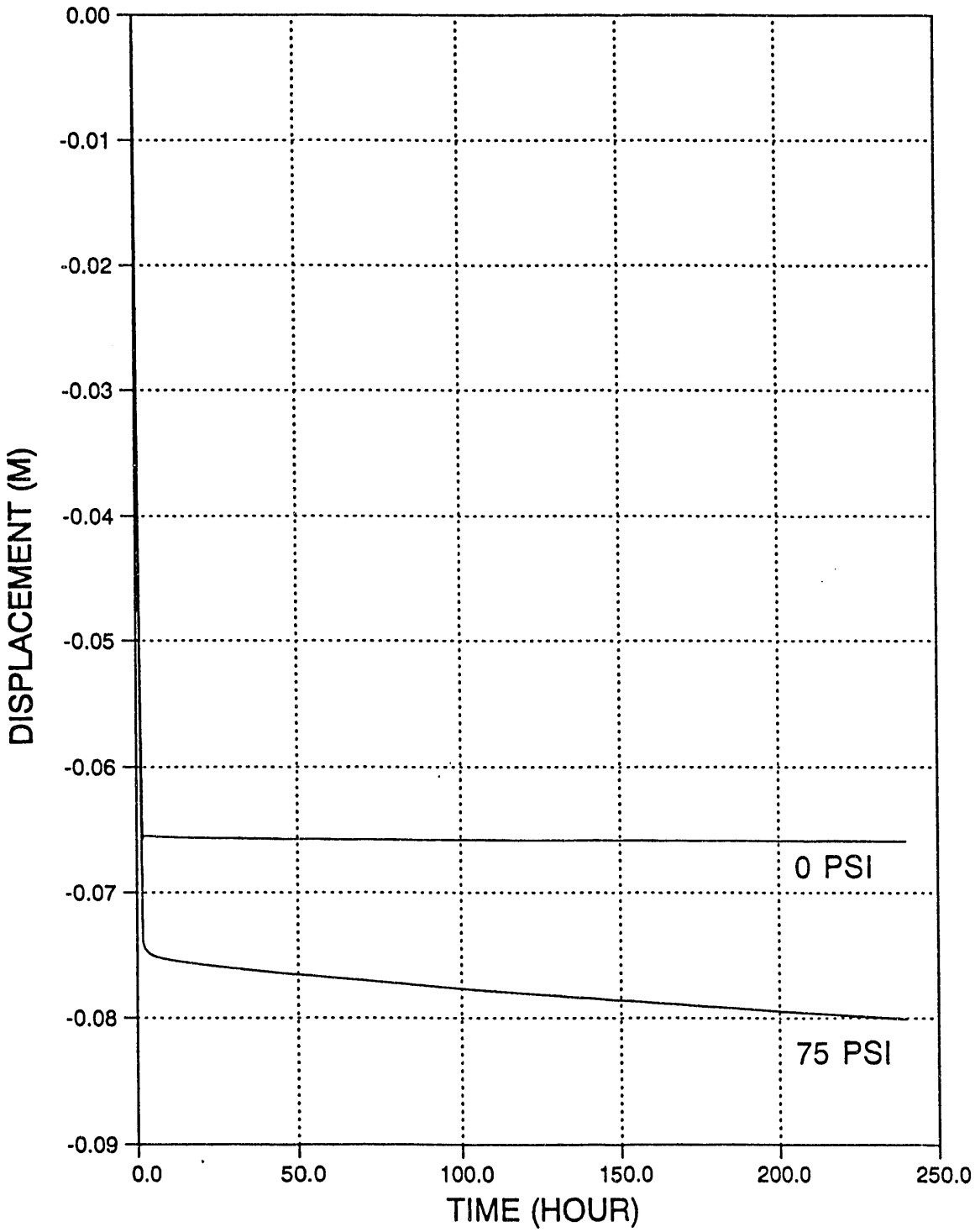
0.00
-0.01
-0.02
-0.03
-0.04
-0.05
-0.06
-0.07
-0.08
-0.09
DISPLACEMENT (M)
0 PSI
75 PSI
0.0
50.0
100.0
150.0
200.0
250.0
TIME (HOUR)

Fig. 22

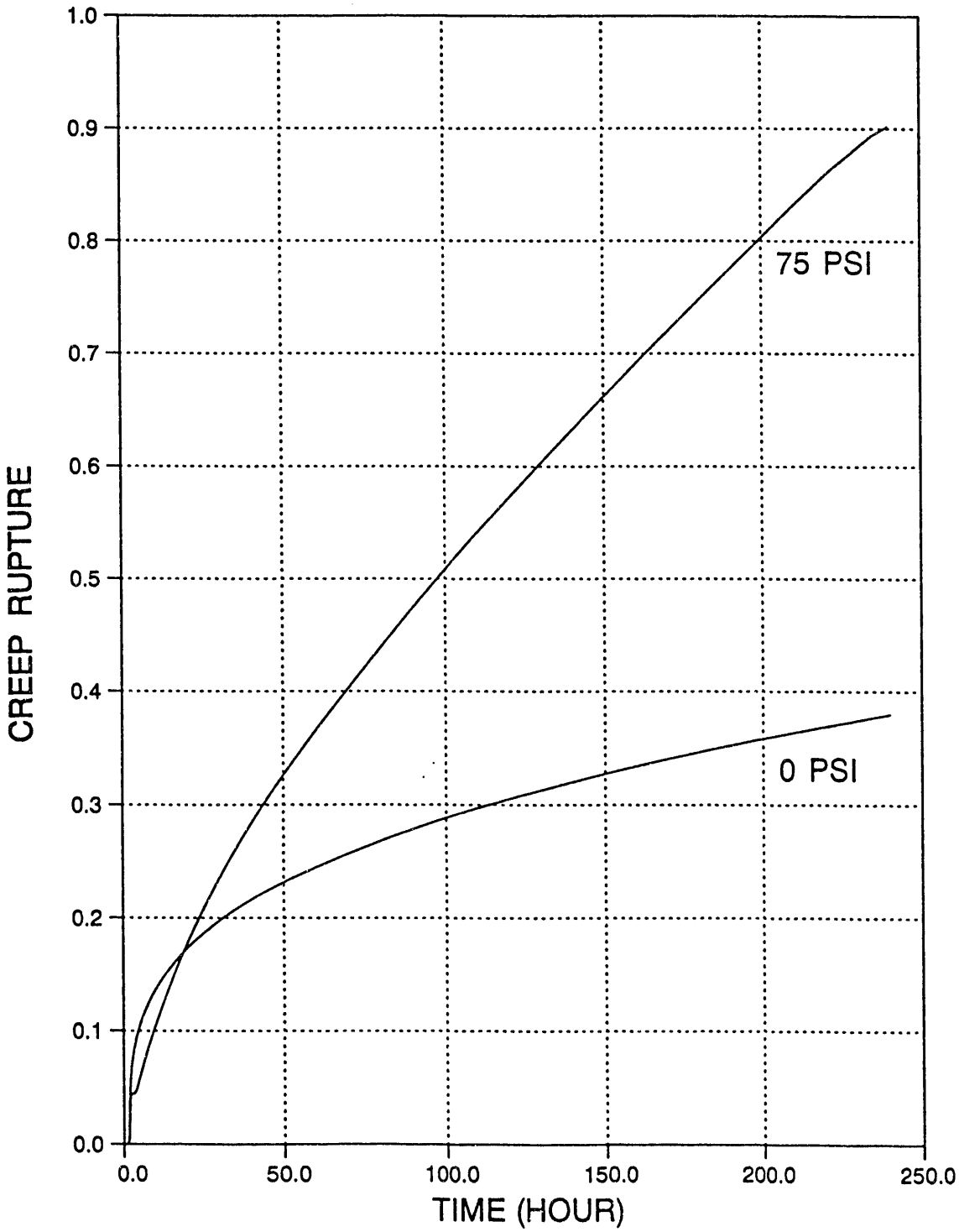
1.0
0.9
0.8
0.7
0.6
0.5
0.4
0.3
0.2
0.1
0.0
CREEP RUPTURE
75 PSI
0 PSI
0.0
50.0
100.0
150.0
200.0
250.0
TIME (HOUR)

Fig. 23

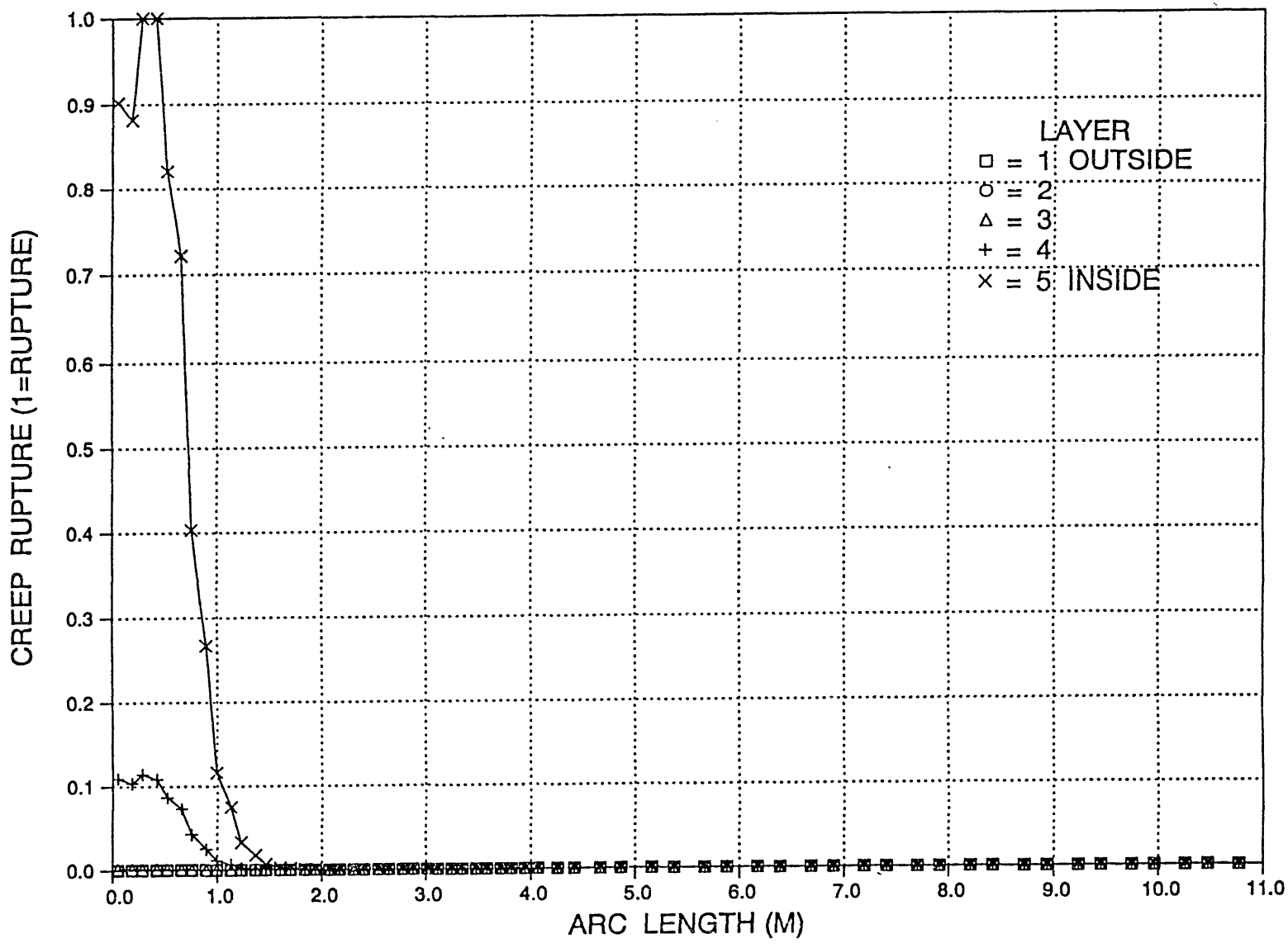
CREEP RUPTURE (1=RUPTURE)
1.0
0.9
0.8
0.7
0.6
0.5
0.4
0.3
0.2
0.1
0.0
0.0
1.0
2.0
3.0
4.0
5.0
6.0
7.0
8.0
9.0
10.0
11.0
ARC LENGTH (M)
LAYER
□ = 1 OUTSIDE
○ = 2
△ = 3
+ = 4
× = 5 INSIDE

Fig. 24

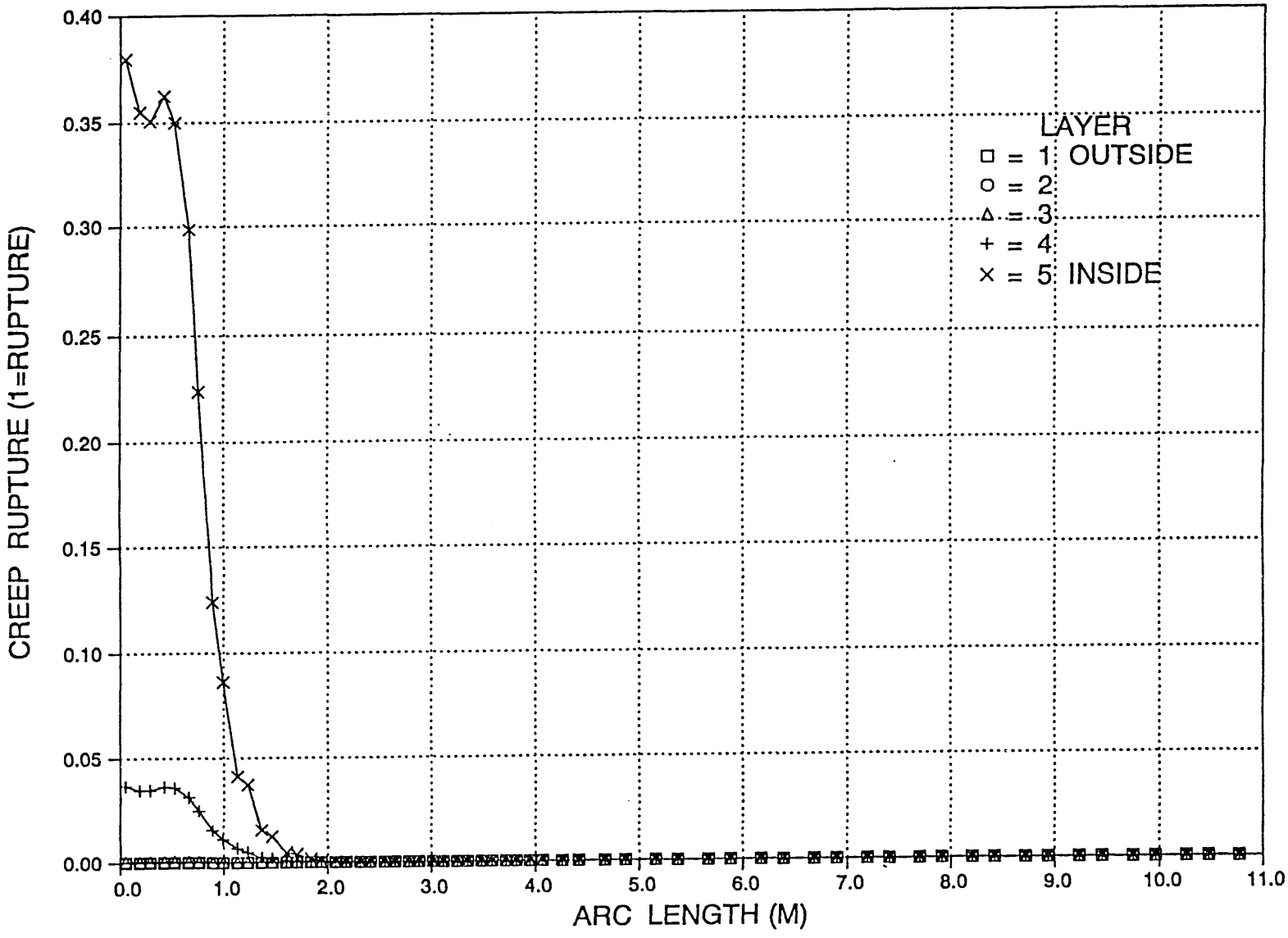
CREEP RUPTURE (1=RUPTURE)
0.40
0.35
0.30
0.25
0.20
0.15
0.10
0.05
0.00
0.0
1.0
2.0
3.0
4.0
5.0
6.0
7.0
8.0
9.0
10.0
11.0
ARC LENGTH (M)
LAYER
□ = 1 OUTSIDE
o = 2
Δ = 3
+ = 4
× = 5 INSIDE

Fig. 25